Model for Acoustic Induced Aluminum Combustion Fluctuations in Solid Rocket Motors

Aurelien Genot, Stany Gallier, Thierry Schuller

A model for acoustic induced aluminum combustion fluctuations in solid rocket motors

Aurelien Genot*
CNES DLA, Centre National d'Etudes Spatiales, Direction des lanceurs, Paris, France

Stany Gallier†
ArianeGroup, Le Bouchet Research Center, Vert-le-Petit, France

Thierry Schuller‡
Laboratoire EM2C, CNRS, CentraleSupélec, Université Paris Saclay, Gif-sur-Yvette, France
Institut de Mécanique des Fluides de Toulouse, IMFT, Université de Toulouse, CNRS, Toulouse, France

Combustion of aluminum droplets released by the solid propellant increases the solid rocket motor thrust. The combustion dynamics of the released droplet cloud in the unsteady flow can trigger thermo-acoustic instabilities. An analytical model for the local heat release rate fluctuations of the burning droplet cloud is derived for small acoustic disturbances. Two contributions to heat release rate fluctuations are identified. The first originates from fluctuations of the evaporation rate due to the oscillating flow around the droplets. This leads to local heat release rate fluctuations within the droplet cloud. The second one lies at the cloud boundary between the burning cloud and the inert zone and is due to droplet lifetime oscillations. Both contributions to heat release rate disturbances take place within the acoustic boundary layer along the solid propellant surface and depend on the droplet diameter, droplet velocity and gas velocity fluctuations. Quasi-steady models for diameter and droplet velocity fluctuations are derived. Model results are compared to a previous low order model and with numerical flow simulations. The derived expressions yield a better understanding on heat release disturbances and can be used to predict the linear stability of a solid rocket motor at reduced computational costs.

I. Nomenclature

α_p = Droplet volume fraction

ΔH_r = Heat of gas reaction (J kg^{-1})

$\dot{m}$ = Droplet mass consumption rate (kg s^{-1})

$\dot{q}$ = Heat release rate (W m^{-3})

*PhD student, CNES/DLA, aurelien.genot@centralesupelec.fr
†Research Engineer, Department of Aerodynamics and Combustion, stany.gallier@ariane.group
‡Professor, thierry.schuller@imft.fr

γ = Specific heat ratio (= $C_{P,g}/C_{V,g}$)

κ = Aluminum mass fraction

$\mathbf{F}$ = Flux vector

$\mathbf{F}_d$ = Drag force (N)

$\mathbf{I}$ = Identity matrix

$\mathbf{P}$ = Stress tensor (N m^{-2})

$\mathbf{S}$ = Source term

$\mathbf{u}$ = Gas velocity vector (m s^{-1})

$\mathbf{u}_p$ = Droplet velocity vector (m s^{-1})

$\mathbf{W}$ = Conservative variable vector

$\mathcal{S}$ = Local Rayleigh source term (W m^{-3})

$\mathcal{H}$ = Heaviside function

$\mathcal{R}e$ = Real part

$\mathcal{I}m$ = Imaginary part

B = Spalding number

Pr = Prandtl number

Sh = Sherwood number

μ = Dynamic viscosity (kg $m^{-1}s^{-1}$)

ω = Angular frequency (= $2\pi f$) (s^{-1})

ρ = Density (kg m^{-3})

τ_v = Drag characteristic time (s)

ξ = Viscous parameter

a = Speed of sound (m s^{-1})

C_P = Specific heat capacity at constant pressure (J kg^{-1} K^{-1})

C_V = Specific heat capacity at constant volume (J kg^{-1} K^{-1})

D = Droplet diameter (m)

d = Distance (m)

E = Total Energy (J)

f = Frequency (Hz)

k = Wavelength (m)

L = Motor chamber length (m)

L_v = Latent heat of vaporization (J kg^{-1})

N_p = Number of particles per unit volume (m^{-3})

p = Gas pressure (Pa)

Q_v = Convective heat flux (W)

R = Motor chamber Radius (m)

r = Radial position / Radius (m)

Re = Reynolds number

S_r = Strouhal number

T = Temperature (K)

u = Axial velocity (m s^{-1})

v = Radial velocity (m s^{-1})

x = Axial position (m)

ψ = Unperturbed acoustic mode shape

$\hat{\eta}$ = Acoustic pressure amplitude (Pa)

Subscripts/Superscripts

0 = Mean quantity

1 = Fluctuations

Al = Aluminum

sat = Saturation conditions

$b.c.$ = Boundary contribution

D^2 = Without Heaviside function

f = Flame

g = Gas phase

i = Injection

Ox = Oxidizer

p = Droplet phase

r = Aluminum oxide residue

rot = Rotational

st = Stoichiometic conditions

t = Throat

$v.c.$ = Volume contribution

$\hat{\cdot}$ = Fluctuations in the Fourier space

n = nth-acoustic mode

ac = Acoustic

l = Acoustic losses

II. Introduction

Flow instabilities in Solid Rocket Motors (SRMs) have been identified in the 1940s [1, 2] and are still a major issue for most motors including Ariane 5 or Ariane 6 programs [3]. Blomshield [4] references a list of instabilities in SRMs, which can alter the chamber pressure, the launcher guidance, the thrust vector control or in the worst cases lead to motor structural failure. Small pressure oscillations in the chamber may lead to high thrust oscillations [5] and all pressure oscillation sources need to be carefully addressed during the design process.

Solid propellant combustion instabilities generally develop in small lab scale motors because the combustion propellant response amplifies flow perturbations at high frequencies [6]. Unsteady solid propellant combustion may couple with pressure or velocity fluctuations [2]. For larger motors, pressure oscillations are often due to hydrodynamic instabilities, as in Ariane 5 segmented boosters [2, 3]. In that case, large scale vortical structures are produced by interactions of the flow with solid protruding obstacles, by changes of the propellant geometry at angles, or in the boundary layer along the solid propellant itself. Vortex transport close to a nozzle cavity [7–9], vortex transport in a contraction (like a nozzle) [10] and vortex shedding [11, 12] are the main pressure oscillation sources.

In aluminized solid propellants, aluminum droplets are released in the chamber [13–15]. These droplets burn and constitute an additional enthalpy to thrust the rocket. As combustion proceeds, the gaseous products released from the burning droplets condense to form an aluminum oxide cap on the droplets that grows in time until combustion is quenched. This finally yields inert droplets. These residual droplets are a source of acoustic losses for pressure oscillations [2, 16] and hinder the development of instabilities coupled to tangential or radial acoustic modes [17]. In the Sentry ballistic missile defense motor [4], aluminum combustion has however been suspected to drive instabilities as well. In Rijke burners, it has been proven experimentally, analytically and numerically that individual burning aluminum droplets can drive thermo-acoustic instabilities [18–20]. Also, many experiments carried out with T-Burners with aluminized propellant develop large pressure pulsations due to the presence of aluminum droplets [21, 22]. The way aluminum droplet combustion couples with the acoustic field remains however unclear.

A series of numerical simulations [23–25] made in a generic SRM helped for a better understanding of the combustion dynamics of aluminum droplets during thermo-acoustic instabilities. These simulations reveal that the dynamics of the burning aluminum droplets released from the solid propellant can couple with one of the low frequency acoustic modes of the motor chamber. Gallier *et al.* [26] demonstrated with a direct numerical flow simulation of a fixed single aluminum droplet with a fixed diameter burning in an oscillating flow, that the burning droplet response is controlled by the unsteady drag exerted by the flow on the evaporation rate of the droplet. Dupays and Vuillot [27] proved that the

mass released from a cloud of vaporizing droplets could drive acoustic waves. To better understand aluminum droplet driven combustion instabilities it is interesting to make a parallel with liquid-fueled systems. The dynamic stability of liquid-fueled powered motors is well known to be altered by the droplet vaporization process [2, 28]. In hydrocarbon fuel spray systems, acoustic oscillations may *(i)* modify the droplet size distribution at the injector inlet [29, 30], *(ii)* segregate large from small droplets during their transport in the pulsed flow [31] and *(iii)* reduce the droplet evaporation time due to the additional drag on the droplets from the pulsed flow [18, 26, 32]. Each of these mechanisms alters the flame dynamics. High-amplitude acoustic oscillations were also found to reduce the length of liquid fuel sprays [33]. Carvalho *et al.* [32] observed a reduction in the mean droplet lifetime due to acoustic forcing in their numerical model of a Rijke tube burning liquid droplets.

This literature survey indicates that the dynamics of an aluminum droplet cloud is likely to be destabilized by the acoustic field and cause thermo-acoustic instabilities in SRMs. This work aims at shedding light on the dynamics of aluminum burning droplets leading to heat release disturbances by taking into account the response of each individual droplets and but also collective effects from the entire droplet cloud when it is submitted to acoustic perturbations.

One examines cases in which heat release rate fluctuations produced by the burning droplets and synchronized by the acoustic field are the main source of thermo-acoustic instabilities in SRMs. It is worth recalling that motors are prone to thermo-acoustic coupling only for very specific conditions, but these conditions are not necessarily met. These undesirable states depend on the phase relationship between pressure and heat release rate disturbances in the motor chamber, the acoustic source and acoustic losses [23]. To simplify the analysis and to highlight possible mechanisms driving a pure thermo-acoustic instability, the other sources of flow instabilities are not considered in this work. The main objective is to derive expressions for the heat release rate fluctuations produced by a cloud of burning droplets released from the propellant and which is submitted to acoustic perturbations. The validity of these expressions is limited to the linear framework to reveal the main mechanisms at the origin of instabilities coupled to the aluminum droplet dynamics. In a real motor, this destabilization mechanism of the thermo-acoustic state of the motor should indeed be considered with the other source instabilities (hydrodynamic instabilities and solid propellant combustion instabilities) that were not taken into account in this paper. It is often considered that the acoustic perturbations with the largest growth rates are the most dangerous ones, but this of course does not presume the final nonlinear state of the motor.

In the next section, a reference numerical flow simulation is carried out in which the flow in a generic SRM is submitted to an acoustic pressure pulsation. This simulation is analyzed to identify the thermo-acoustic sources. The governing equations computed by the flow solver are first described. Results are then analyzed to identify the different contributions to heat release rate fluctuations inside the SRM. Derivation of a low-order linear model for heat release rate disturbances from a cloud of burning aluminum droplets is conducted in section IV. In the same section, comparisons with a previous model from Gallier and Godfroy [23], the numerical flow simulations described in section III and the

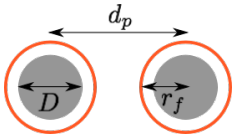

Fig. 1 Two burning droplets of diameter D and flame radius r_f separated by a distance d_p.

new model are presented. It is demonstrated that acoustic fluctuations lead to droplet velocity and droplet diameter disturbances and that both contributions need to be considered to reproduce the correct level and phase lag of heat release rate fluctuations observed in the numerical flow simulations.

III. Reference simulation

A. About group combustion for aluminum

Aluminum combustion is usually assumed to take place in SRM in a distributed mode [19, 34]. However, the combustion regime depends on the droplet volume fraction. Group combustion effects are customarily evaluated with Chiu's approach [35, 36]. Nakamura *et al.* [37] identified two regimes of two-phase flow combustion, a premixed-like combustion mode and a diffusion-like combustion mode. In a premixed-like combustion regime, the oxidizer is initially present around each individual droplet whereas in a diffusion-like combustion mode, the oxidizer is only present at the boundary of the droplet cloud. For premixed-like combustion, Chiu's criterion overestimates the group behavior because it does not take into account the effect of the initial oxygen concentration [37, 38].

Aluminum droplets are injected in SRMs with the gas products exhausting from the solid propellant combustion that are mainly composed of CO_2, H_2O, CO and N_2. The combustion reaction takes place between the aluminum droplets and the oxidizers CO_2 and H_2O [19]. Initially, at the injection surface, each aluminum droplet is surrounded by the oxidizer gas and therefore aluminum combustion can be classified as a premixed-like combustion regime. In this case, Chiu's approach is not relevant to validate the assumption of isolated burning aluminum droplets. It is better to consider the mean inter-particle distance d_p compared to the droplet flame radius r_f as illustrated in Fig. 1 [34, 39]. From percolation theory, a limit for isolated burning droplet may be derived [40]:

$$\frac{r_f}{d_p} < 0.43 \tag{1}$$

The mean inter-particle distance d_p can be evaluated as a function of the volumetric fraction α_p of droplets in the propellant and the droplet diameter D [34]:

$$\frac{d_p}{D} = \left(\frac{6\alpha_p}{\pi}\right)^{-1/3} \tag{2}$$

Aluminum droplets being oxidized by two reactants CO_2 and H_2O, it is difficult to get reliable estimates of the flame radius r_f from theory [40]. It has been decided in this study to refer to experiments to evaluate r_f. The measurements

from Bucher *et al.* [41, 42] yield:

$$\frac{r_f}{D} \simeq 3 \tag{3}$$

One third of the initial mass of aluminum within the propellant forms droplet agglomerates [43]. Because of their small size, we assume that the remaining aluminum particles burn very close to the surface of the solid propellant and are neglected in the present analysis [23]. So, for a propellant loaded with a mass fraction of $Y_{Al} = 0.18$ of aluminum, only a mass fraction $\kappa = 0.06$ of aluminum droplets released in the gas are considered. In these conditions, the volumetric fraction α_p of droplets and the ratio r_f/d_p are equal to:

$$\alpha_p = 3.\,10^{-4} \ll 1 \quad \text{and} \quad \frac{r_f}{d_p} = 0.25 < 0.43 \tag{4}$$

The fraction α_p remaining small, a dilute particle phase is assumed. The ratio r_f/d_p is also small enough to neglect group combustion effects and consider a distributed combustion of droplets burning individually.

B. Governing equations

A single class of spherical droplets, burning individually, is considered. The impact of polydispersity of the droplet cloud is expected to be a second order effect on the system stability. It could potentially alter the instability levels but may not change the physical mechanisms. Simulations are carried out by solving the compressible Navier-Stokes equations with the perfect gas law, in a two-way coupling Eulerian framework using Marble's two-phase flow model [23, 44]. This yields the following system of conservation equations:

$$\frac{\partial}{\partial t}\begin{pmatrix}\mathbf{W_g}\\ \mathbf{W_p}\end{pmatrix} + \nabla\cdot\begin{pmatrix}\mathbf{F_g}\\ \mathbf{F_p}\end{pmatrix} = \begin{pmatrix}\mathbf{S_g}\\ \mathbf{S_p}\end{pmatrix} \tag{5}$$

where $\mathbf{W_g}$ and $\mathbf{W_p}$ denote the conservative variable vectors for the gas phase and the droplet phase respectively:

$$\mathbf{W_g} = \begin{pmatrix}\rho_g\\ \rho_g\mathbf{u}\\ \rho_g E_g\end{pmatrix}, \quad \mathbf{W_p} = \begin{pmatrix}\rho_p\alpha_p\\ \rho_p\alpha_p\mathbf{u}_p\\ \rho_p\alpha_p E_p\\ N_p\end{pmatrix} \tag{6}$$

The mass, momentum and energy flux vectors $\mathbf{F_g}$ and $\mathbf{F_p}$ for each phase are:

$$\mathbf{F_g} = \begin{pmatrix} \rho_g \mathbf{u} \\ \rho_g \mathbf{u} \otimes \mathbf{u} - \mathbf{P} \\ \rho_g \mathbf{u} E_g - \mathbf{P} \cdot \mathbf{u} \end{pmatrix}, \quad \mathbf{F_p} = \begin{pmatrix} \rho_p \alpha_p \mathbf{u}_p \\ \rho_p \alpha_p \mathbf{u}_p \otimes \mathbf{u}_p \\ \rho_p \alpha_p \mathbf{u}_p E_p \\ \mathbf{u}_p N_p \end{pmatrix} \tag{7}$$

The mass, momentum and energy source term vectors $\mathbf{S_g}$ and $\mathbf{S_p}$ are:

$$\mathbf{S_g} = \begin{pmatrix} N_p \dot{m} \\ N_p \dot{m} \mathbf{u_p} - \mathbf{F_d} \\ N_p \dot{m} (E_p + L_v + \Delta H_r) - Q_v - \mathbf{F_d} \cdot \mathbf{u_p} \end{pmatrix}, \quad \mathbf{S_p} = \begin{pmatrix} -\mathbf{S_g} \\ 0 \end{pmatrix} \tag{8}$$

In these expressions, $\otimes$ is the tensor product, ρ_g the gas density, ρ_p the aluminum droplet material density which is assumed to remain constant, $\mathbf{u}$ the gas velocity, $\mathbf{u}_p$ the droplet velocity, E_g the gas total energy, E_p the particle total energy, N_p the number of particles per unit volume (coalescence and breakup are not considered), $\dot{m}$ the individual droplet mass consumption rate, L_v the latent heat of vaporization, ΔH_r the heat of gas reaction, Q_v the convective heat flux conferred by the hot gases to the droplet, $\mathbf{F}_d$ the drag force acting on the droplets and $\mathbf{P}$ the stress tensor of a Newtonian fluid which is given by:

$$\mathbf{P} = -p\mathbf{I} + \mu \left(\nabla \mathbf{u} + \nabla \mathbf{u}^T - \frac{2}{3} (\nabla \cdot \mathbf{u}) \mathbf{I} \right) \tag{9}$$

with p the gas pressure, μ the dynamic gas viscosity and $\mathbf{I}$ the identity matrix.

In this model, droplets have the same diameter D in each computational cell given by:

$$D = \left(\frac{6\alpha_p}{\pi N_p} \right)^{1/3} \tag{10}$$

Modelling droplet aluminum combustion is a difficult problem. The D^2-law [45, 46] only gives a rough approximation of the evaporation rate of an aluminum droplet. A deviation from the D^2-law is observed due to the formation of an aluminum oxide cap [19, 47, 48]. The D^2-law is used here as first approximation to get insight on the response of a burning cloud of aluminum droplets transported by a flow and submitted to acoustic oscillations. The droplet mass

release rate $\dot{m}_{D^2}$ is, under unit Lewis number assumption, modeled by:

$$\dot{m}_{D^2} = \pi D \frac{\mu}{\mathrm{Pr}} \ln(1 + \mathrm{B})\mathrm{Sh} \tag{11}$$

where Pr is the Prandtl number, Sh the Sherwood number and B the thermal Spalding number expressed as [23]:

$$\mathrm{B} = \frac{C_{P,g}(T_g - T_p) + \Delta H_r}{L_v} \tag{12}$$

with $C_{P,g}$ the gas specific heat capacity at constant pressure, T_g the gas temperature and T_p the droplet temperature. To take into account the formation of inert aluminum oxide as combustion comes to its end [19, 24], combustion is abruptly quenched when the droplet diameter falls below a critical value D_r [49]. The droplet mass release is finally defined as:

$$\dot{m} = \dot{m}_{D^2}\mathcal{H}(D - D_r) \tag{13}$$

where $\mathcal{H}$ is the Heaviside function. The droplets with diameters $D = D_r$ model the inert aluminum oxide residues that persist in the flow after combustion is quenched. Note that this model is only valid for large aluminum oxide residues. The Heaviside function is used here to model the disruptive combustion end behavior of individual aluminum burning droplets (explosions, jetting effects) as seen in some experiments [13, 19, 50]. The aluminum oxide smoke resulting from combustion is not considered in this work [19].

Direct numerical flow simulations of a fixed burning aluminum droplet in an oscillating flow revealed that the droplet response to the pulsation is controlled by the convection around the droplet [26]. This response is well modeled by the Ranz-Marshall correlation [26, 51]. In the following simulations, the Sherwood number follows the Ranz-Marshall correlation:

$$\mathrm{Sh} = 2 + 0.6\mathrm{Re}_p^{1/2}\mathrm{Pr}^{1/3} \tag{14}$$

where the droplet Reynolds number is defined as:

$$\mathrm{Re}_p = \frac{\rho_g |\delta\mathbf{u_p}| D}{\mu} \quad \text{with} \quad \delta\mathbf{u_p} = \mathbf{u}_p - \mathbf{u} \tag{15}$$

in which $\delta\mathbf{u_p}$ is the relative droplet velocity with respect to the gaseous stream. The drag force $\mathbf{F}_d$ acting on a spherical and burning droplet is modeled by Schiller and Naumann correlation [23, 52]:

$$\mathbf{F}_d = -\frac{18\mu\alpha_p \left(1 + 0.15Re_p^{0.687}\right)}{D^2(1 + \mathrm{B})}\delta\mathbf{u_p} \tag{16}$$

The Biot number being small, aluminum droplets are assumed isothermal during their combustion. The droplet

temperature is taken equal to the saturation temperature of aluminum $T_p = T_{sat}$. To be consistent, it is also assumed that all the convective heat flux Q_v from the hot gases is used to sustain droplet evaporation:

$$Q_v = N_p \dot{m} L_v \tag{17}$$

This approximation simplifies the source terms $\mathbf{S_g}$ and $\mathbf{S_p}$ in Eq. (8). When the droplet diameter reaches the critical value $D = D_r$, the convective heat flux Q_v around inert aluminum oxide particles is modeled as in [23]. In this framework, the volumetric heat release rate due to aluminum combustion corresponds to:

$$\dot{q} = N_p \dot{m} \left(\Delta H_r + C_{V,p} T_p - C_{V,g} T_g + \frac{\delta \mathbf{u_p}^2}{2} \right) \tag{18}$$

where $\delta \mathbf{u_p}$ the relative droplet velocity vector, $C_{V,p} = C_{P,p}$ denotes the droplet specific heat capacity and $C_{V,g}$ stands for the gas specific heat capacity at constant volume. One also defines $\dot{q}_{D^2}$ the heat release rate that would be produced if combustion had proceed until complete evaporation of aluminum droplets. In this case, the aluminum mass consumption rate $\dot{m}$ defined by Eq. (13) with aluminum oxide is replaced in Eq. (18) by $\dot{m}_{D^2}$ given by Eq. (11):

$$\dot{q}_{D^2} = N_p \dot{m}_{D^2} \left(\Delta H_r + C_{V,p} T_p - C_{V,g} T_g + \frac{\delta \mathbf{u}_p^2}{2} \right) \tag{19}$$

C. Numerical modeling

Simulations are made with CPS, an in-house ArianeGroup flow solver [53]. The numerical model used to solve the previous equations is described in [23–25]. The governing equations are discretized and resolved by a finite volume technique adapted to unstructured meshes. The numerical schemes are second order accurate in space (Monotonic Upwind Scheme for Conservation Laws) and second order accurate in time using explicit two-step Runge-Kutta time stepping. The time step is limited by a Courant-Friedrichs-Lewy condition set to CFL= 0.55.

Simulations shown in this work are carried out in a 2D axisymmetric framework. The configuration explored in Fig. 2 is a cylindrical motor, with radial injection of mass at the boundary $R = 0.593$ m. This mass injection models the gas and aluminum droplet released by the solid propellant combustion. The solid propellant burning velocity is neglected and the geometry is fixed in these simulations because the flow velocity is much higher than the solid propellant burning velocity over the simulated period. The chamber has a radius $R = 0.593$ m, a length $L = 7$ m and a symmetry axis at $r = 0$. The flow exhausts through a chocked nozzle with a throat of radius $R_t = 0.175$ m, which is located at $x_t = 7.3$ m away from the motor head-end $x = 0$. The motor head-end corresponds here to a flat solid wall.

The computational grid is composed of 360,000 quads with about 600 points in the axial direction and 600 points in the radial direction. The grid is clustered near the propellant burning surface to resolve the aluminum distributed

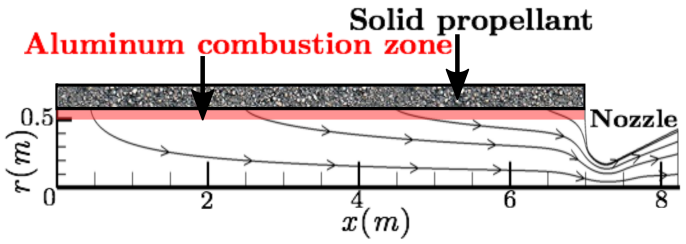

Fig. 2 Solid rocket motor schematic. Aluminum droplet combustion is delineated by the red zone. A few gas streamlines of the steady flow are also plotted.

combustion. The region where aluminum combustion reaction takes place is indicated in red in Fig. 2. It corresponds to a thin region in the boundary layer of the solid propellant. The smallest grid spacing at the propellant surface is about 0.1 mm and the mesh is refined in the aluminum combustion region. Outside the aluminum combustion region particles are inert.

Turbulence is not taken into account in these simulations to focus the analysis on the coupling between acoustics and unsteady aluminum droplet combustion [23, 54] without dealing with the complexity of interactions with turbulence. Grid convergence has been checked and no significant differences have been found between results calculated with this grid and a coarser mesh with 172,000 quads.

No-slip conditions are used for the gaseous and particle phases at the wall boundaries including the head-end and the nozzle. Solid propellant burning is modeled through the lateral boundary of the numerical domain between $x = 0$ and L by injection of hot burnt gases at a constant mass flow rate with a velocity vector normal to the surface and pointing inwards. Gas and aluminum droplets are injected radially at the same velocity $v_{p,i} = v_i$. The mass flux of the two-phase droplet and gaseous mixture released from the solid propellant combustion is set to $(\rho v)_i = 24.6$ kg.m^{-2}.s^{-1}. Considering only the aluminum agglomerates, the mass fraction of injected aluminum droplet is set to $\kappa_i = 0.06$ [43]. The response of the solid propellant combustion rate to acoustic oscillations is not considered here to focus the analysis on aluminum droplet combustion driven instabilities.

Aluminum droplets have an initial diameter $D_i = 120$ μm corresponding to aluminum agglomerates and the aluminum oxide residue diameter is fixed to $D_r = 50$ μm [24, 43, 55]. Aluminum particles are injected from the solid propellant surface at the saturation temperature $T_{p,i} = T_{sat} = 2791$ K. The injected gas is at the temperature $T_{g,i} = 3440$ K. The specific heat capacity at constant pressure of the gaseous phase is fixed to $C_{P,g} = 1997$ J kg^{-1} K^{-1} and to $C_{P,p} = 1177$ J kg^{-1} K^{-1} for the aluminum droplets [27]. The specific heat capacity ratio of the gas is $\gamma = \frac{C_{P,g}}{C_{V,g}} = 1.16$. The latent heat of aluminum droplet vaporization is $L_v = 10.8 \times 10^6$ J kg^{-1} and the heat of reaction per unit mass, after vaporization, is $\Delta H_r = 9.53 \times 10^6$ J kg^{-1}. Gas and aluminum droplet properties used in these simulations are summarized in Table 1.

Table 1 Gas and aluminum droplet properties in the SRM

μ	9.1×10^{-5} kg m^{-1} s^{-1}	Pr	0.4
D_i	120 μm	D_r	50 μm
$(\rho v)_i$	24.6 kg m^{-2} s^{-1}	ΔH_r	9.53×10^6 J kg^{-1}
κ_i	6%	L_v	10.8×10^6 J kg^{-1}
$T_{g,i}$	3440 K	T_{sat}	2791 K
$C_{P,g}$	1997 J kg^{-1}.K^{-1}	$C_{P,p}$	1177 J kg^{-1} K^{-1}
γ	1.16	f	70.45 Hz
$\hat{\eta}$	4200 Pa		

D. Simulation results

The configuration investigated is thermo-acoustically stable, meaning that no-self sustained oscillation naturally develops in the SRM. Acoustic excitation is imposed at the head-end boundary at $x = 0$ with a pressure pulsation of amplitude $\hat{\eta} = 4200$ Pa locked on the first longitudinal mode of the SRM at the frequency $f = 70.45$ Hz. The resulting acoustic field is a standing wave in the SRM with hard wall acoustic boundaries at both extremities. The first extremity is at $x = 0$ and the second one corresponds to the throat of the chocked nozzle at $x = 7.3$ m.

The selected forcing frequency $f = 70.45$ Hz corresponds to the frequency of the limit cycle of the unstable case studied in [24, 25] when the residual diameter of aluminum particles is fixed to $D_r = 60$ μm. The pressure pulsation level $\eta = 4200$ Pa chosen to excite the system corresponds to half the pressure level observed at this limit cycle. It was checked that this forcing level $\hat{\eta}/p_0 = 4.\,10^{-4}$ is small enough compared to the mean pressure $p_0 \simeq 100$ bar to get linear pressure and heat release rate fluctuations in this study.

The response of the heat release rate due to aluminum combustion is shown in Fig. 3 at four regularly distributed instants in a forcing cycle. The timing between each instant is $T/4 \approx 3.5 \times 10^{-3}$ s, with $T = 1/f$ the acoustic period. The axes are stretched in the radial direction in this figure. The view frame is zoomed over the aluminum combustion zone shown in red in Fig. 2. Aluminum droplets are injected at $r/R = 1$ and a few droplet streamlines are indicated in Fig. 3 with blue arrows. They show that the droplets cross the combustion region with a quasi-radial trajectory. Droplet diameter change along a streamline is also indicated.

Figure 3 reveals axial fluctuations of the volumetric heat release rate $\dot{q}$ throughout the combustion volume. This contribution is associated to disturbances of the individual combustion rate of aluminum droplets due to the axial acoustic velocity fluctuations imposed to the flow as described in [23, 26].

The second striking feature in Fig. 3 is a flapping motion of the combustion volume boundary corresponding to the region where the aluminum droplet diameter has reached its critical value $D = D_r$ separating the combustion zone with $D > D_r$ from the zone filled with inert aluminum oxide particles with diameter D_r. This motion takes essentially place in the radial direction while the acoustic mode is controlled by an axial oscillation of the flow. It has recently been

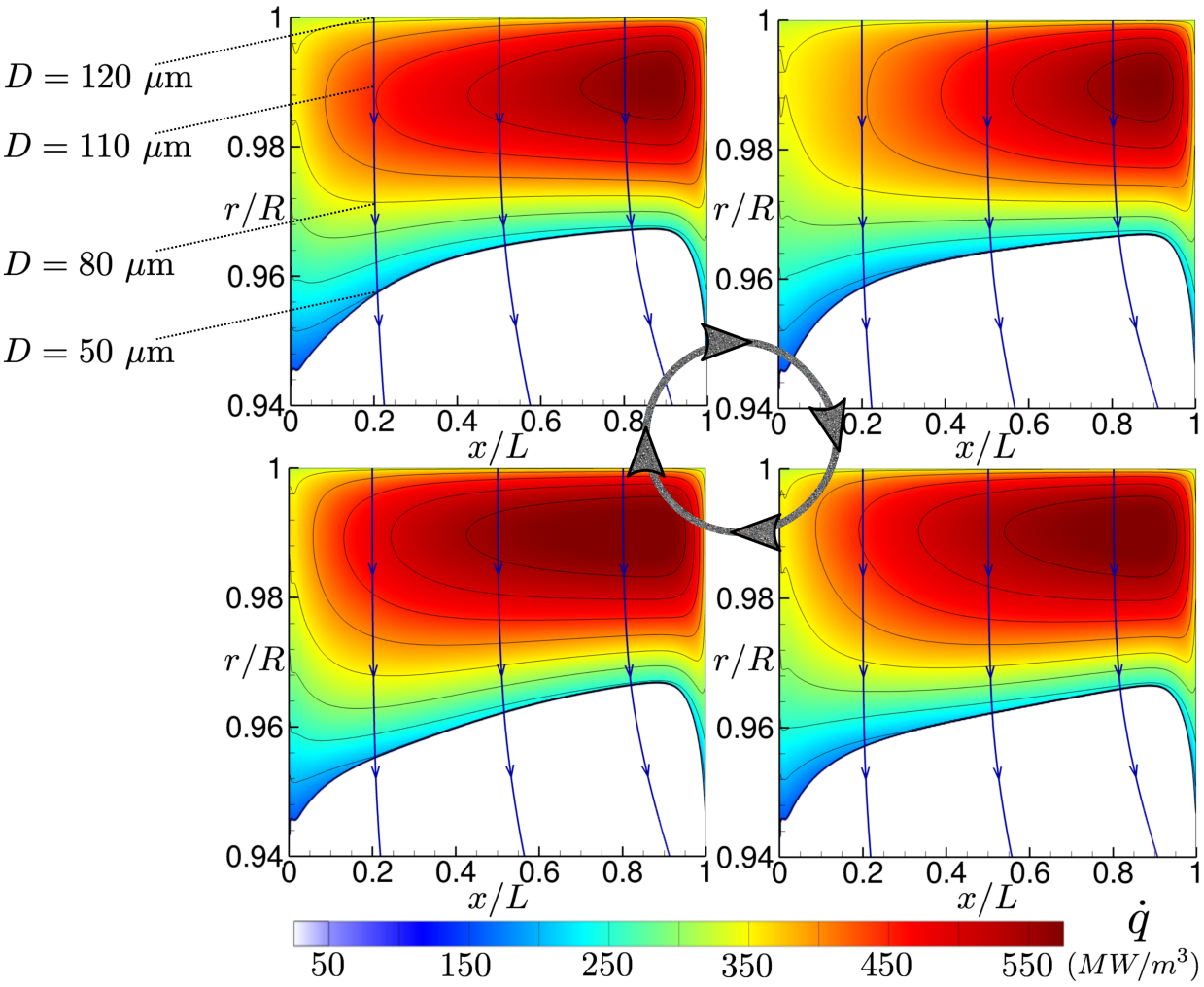

Fig. 3 Heat release rate $\dot{q}$ from aluminum combustion at four instants in an oscillation cycle at $f = 70.45$ Hz. The blue arrows correspond to few droplet streamlines.

shown that this motion originates from droplet lifetime oscillations [25].

Figure 4(a) shows the heat release rate distribution $\dot{q}_{\hat{\eta}=0}$ without acoustic forcing ($\hat{\eta} = 0$). This distribution is compared to that in Fig. 4(b) corresponding to the heat release rate averaged over the forcing cycle $\dot{q}_0 = \frac{1}{T}\int_T \dot{q}dt$, where $T = 1/f$ is the acoustic forcing period. The forcing frequency is $f = 70.45$ Hz and the pressure fluctuation amplitude is fixed to $\hat{\eta} = 4200$ Pa at the head-end of the SRM. Away from the boundary of the combustion zone, the distribution of the heat release rate and the oscillation level reached by the flow are the same in both images. Differences are observed near the combustion end zone, where the boundary is flapping in Fig. 3. This corresponds to the blue zone in Fig. 4(b). Nonlinear effects need to be considered in this region because the mean volumetric rate of heat released changes with the acoustic pressure amplitude.

All the following results correspond to the forced simulation with $\hat{\eta} = 4200$ Pa and $f = 70.45$ Hz. To illustrate the response of aluminum combustion to acoustic oscillations, Fig. 5(a) shows the modulus of the resulting heat release rate

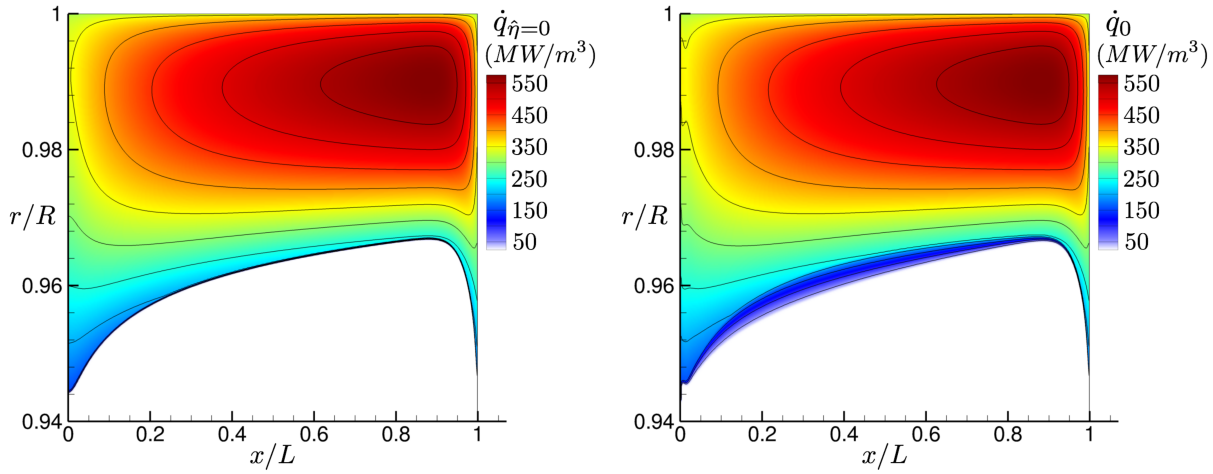

(a) $\hat{\eta}$ = 0**, without acoustic forcing** **(b)** $\hat{\eta}$ = 4200 **Pa, forced simulation**

Fig. 4 Volumetric heat release rate distribution due to aluminum combustion. (a) : $\dot{q}_{\hat{\eta}=0}$ **without acoustic forcing. (b) :** $\dot{q}_0$ **averaged over the acoustic forcing cycle.**

fluctuations $|\hat{\dot{q}}|$ in the SRM. As in Fig. 3, relatively small fluctuations of the volumetric heat release rate $|\hat{\dot{q}}|$ can be identified in blue throughout the combustion volume in Fig. 5(a). These contributions are designated as the volumetric contribution. Higher fluctuation levels of the heat release rate are observed at the boundary of the combustion volume. The motion of this boundary leads to large heat release rate fluctuations that are designated in this work as the boundary contribution. While large differences are observed for heat release rate disturbances in the volume and at the boundary of the aluminum combustion zone, coupling with acoustic pressure needs also to be considered.

Sound production in a thermo-acoustic instability is due to the coupling between pressure and heat release rate fluctuations, which are here associated to unsteady aluminum particle combustion. To highlight this coupling, the local Rayleigh source term $\mathcal{S}$ appearing in the acoustic energy balance is plotted in Fig. 5(b) :

$$\mathcal{S} = \frac{\gamma - 1}{\gamma p_0 T} \int_T p_1 \dot{q}_1 dt \tag{20}$$

The red colors in this figure correspond to positive values of the Rayleigh source term $\mathcal{S}$ and are associated to regions of the flow characterized by sound production. The blue colors correspond to the negative values for $\mathcal{S}$ and are associated to regions of the flow with acoustic damping. Figure 5(b) shows that unsteady aluminum droplet combustion at the head-end destabilizes the system, while the combustion taking place close to the nozzle stabilizes the SRM. The sign of $\mathcal{S}$ also depends on the acoustic mode which is considered and which is here the first longitudinal mode of the SRM. High contributions to $\mathcal{S}$ are visible in the volume and at the boundary in the flapping region in Fig. 5(b), indicating that both volumetric and boundary contributions to heat release rate fluctuations identified in Fig. 5(a) need to be considered

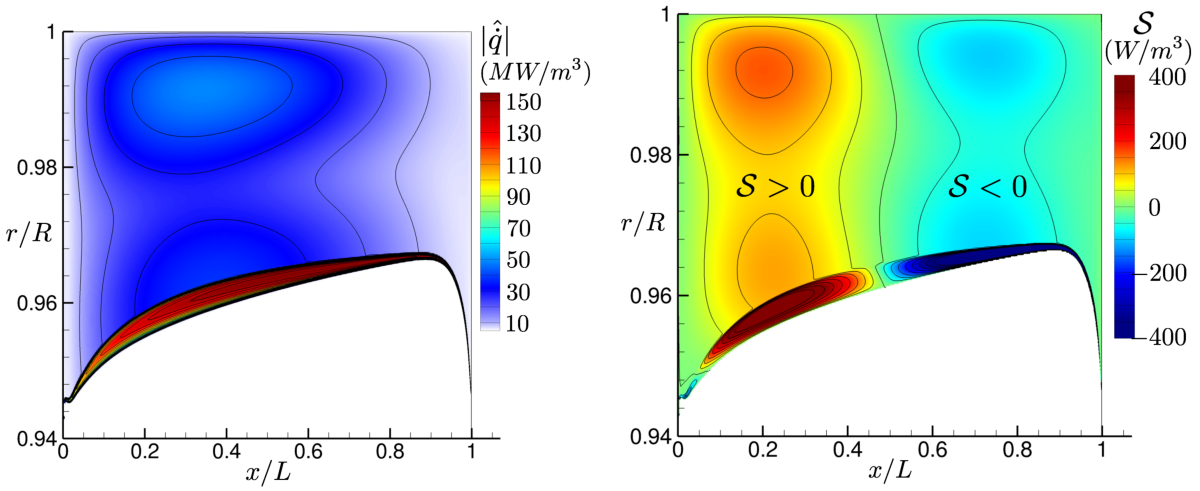

(a) $|\hat{\dot{q}}|$ **(b)** $\mathcal{S} = \frac{\gamma-1}{\gamma p_0 T} \int_T p_1 \dot{q}_1 dt$

Fig. 5 (a) Modulus of heat release rate fluctuations $|\hat{\dot{q}}|$ and (b) local Rayleigh source term $\mathcal{S}$.

in the production/damping of sound by unsteady aluminum combustion. By integration of $\mathcal{S}$, the boundary contribution is about 25% and the volumetric contribution 75% of the thermo-acoustic source $\int_V \mathcal{S} dV$, with V the chamber volume.

Due to the no-slip condition at the solid propellant boundary $r/R = 1$, viscous dissipation alters the fluctuations in a thin region near the solid propellant surface. With a radial gas injection at $r/R = 1$, the acoustic boundary layer is relatively thick and has a very peculiar structure [2, 56–58]. Vorticity waves are created, distort the acoustic waves and modify the gas velocity fluctuations in the acoustic boundary layer of the forced flow [56]. Outside this region, vortical effects are negligeable [59]. The structure of this acoustic boundary layer calculated with CPS is illustrated by plotting the modulus of the axial gas velocity fluctuation $\hat{u}$ in Fig. 6 at a distance $x/L = 1/4$ corresponding to the quarter of the SRM with respect to the chamber head-end. Results are normalized in this figure by the acoustic velocity fluctuation $\hat{u}_{ac}$ that settles along the SRM axis. This value would be reached throughout the entire cross section of the motor $\hat{u} = \hat{u}_{ac}$ for an inviscid flow. This figure shows that aluminum combustion takes place within this acoustic boundary layer. As a consequence, the structure of this acoustic boundary layer has to be taken into account to understand the response of burning aluminum droplets to flow disturbances.

IV. Linear aluminum combustion response model

Due to the small size of the droplets and the low forcing frequencies investigated in this work, the droplet response to acoustic perturbations is assumed to be quasi-steady [26, 29, 60]. This property is used in the following to develop an unsteady combustion model with the same quasi-steady approximation and by linearizing the governing equations shown in section III.B around the mean flow.

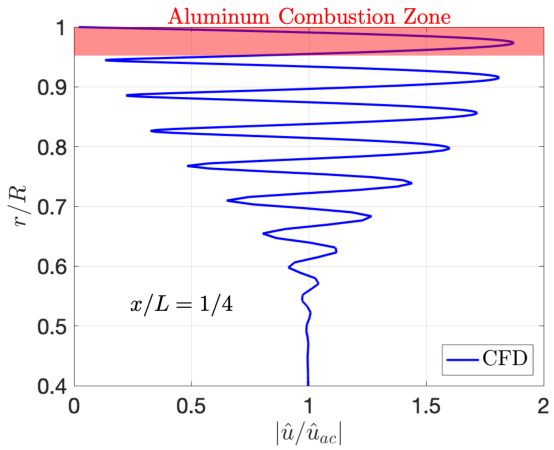

Fig. 6 Velocity fluctuations in the acoustic boundary layer of the SRM at $x/L = 1/4$. The zone covered by aluminum combustion is emphasized in red.

As the system is submitted to acoustic harmonic forcing at frequency f, all signals of the physical variables are assumed to be also harmonic at the same frequency. The signal X is decomposed as $X = X_0 + X_1$, where the mean is given by:

$$X_0 = \frac{1}{T}\int_T X dt \tag{21}$$

with $T = 1/f$ the acoustic period. The subscript 1 stands for the perturbed state around the mean value designated by the subscript 0. The Fourier transform corresponds to:

$$\hat{X} = \int_T X \exp(-i\omega t) dt \quad \omega = 2\pi f \tag{22}$$

where $\hat{\cdot}$ stands for the Fourier component of the perturbation and the inverse Fourier transform yields the disturbance:

$$X_1 = \mathcal{R}e\left(\hat{X}\exp(i\omega t)\right) \tag{23}$$

The model for heat release rate disturbances produced by acoustic pulsations from Gallier and Godfroy [23] is briefly recalled and results are compared to direct numerical flow simulations. Analytical developments are then carried out to better model the droplet dynamics and the resulting heat release rate disturbances by considering fluctuations of the droplet diameter and the motion of the aluminum combustion boundary of the pulsed flow.

A. Model from Gallier and Godfroy [23]

In Appendix A of [23], Gallier and Godfroy derived an expression for the heat release rate disturbances $\hat{q}$ produced by burning aluminum droplets when they are submitted to acoustic pulsations. This model is based on the assumption that the heat release rate fluctuations from the burning droplet cloud result from the flame fluctuations of each individual

droplet in the perturbed flow.

Their analysis relies on the same governing equations as in this study. They first demonstrated that heat release rate fluctuations $\hat{\dot{q}}$ overwhelm the drag force work and kinetic energy fluctuations in the production of pressure oscillations. A perturbation analysis of Eq. (18) leads in this case to :

$$\hat{\dot{q}} = \widehat{N_p \dot{m}} \left(\Delta H_r + C_{V,p} T_{sat} - C_{V,g} T_{g,0} + \frac{|\delta \mathbf{u_p}|_0^2}{2} \right) \tag{24}$$

where fluctuations of the reaction heat are also neglected. The corresponding mean heat release rate $\dot{q}_0$ is given by:

$$\dot{q}_0 = N_{p,0} \dot{m}_0 \left(\Delta H_r + C_{V,p} T_{sat} - C_{V,g} T_{g,0} + \frac{|\delta \mathbf{u_p}|_0^2}{2} \right) \tag{25}$$

Fluctuations are made dimensionless :

$$\frac{\hat{\dot{q}}}{\dot{q}_0} = \frac{\hat{N}_p}{N_{p,0}} + \frac{\hat{\dot{m}}}{\dot{m}_0} \tag{26}$$

Relative fluctuations of the droplet number density $\hat{N}_p / N_{p,0}$ are second order terms with respect to fluctuations of the mass burning rate $\hat{\dot{m}}/\dot{m}_0$ [23]. Neglecting droplet diameter fluctuations $\hat{D}$, gas temperature fluctuations $\hat{T}_g$, gas density fluctuations $\hat{\rho}_g$, radial flow $\hat{v}$ and droplet $\hat{v}_p$ velocity fluctuations [23, 57], linearization of $\dot{m}$ in Eq. (13) yields:

$$\frac{\hat{\dot{q}}}{\dot{q}_0} = \frac{\hat{\dot{m}}}{\dot{m}_0} = \frac{\mathrm{Sh}_0 - 2}{2\mathrm{Sh}_0} \frac{\delta u_{p,0}}{|\delta \mathbf{u_p}|_0^2} (\hat{u}_p - \hat{u}) \tag{27}$$

In this model, heat release rate fluctuations $\hat{\dot{q}}$ solely result from axial droplet velocity $\hat{u}_p$ and axial gas velocity $\hat{u}$ fluctuations. The droplet velocity fluctuations $\hat{u}_p$ can be expressed as a function of the gas velocity fluctuations $\hat{u}$. Combining the momentum conservation with the mass conservation of the droplet phase (Eqs. (5)–(8)) leads to the following transport equation along the axial direction for the droplet velocity:

$$\frac{\partial u_p}{\partial t} + u_p \frac{\partial u_p}{\partial x} + v_p \frac{\partial u_p}{\partial r} = -\frac{\delta u_p}{\tau_v} \tag{28}$$

where τ_v is the droplet drag characteristic time:

$$\tau_v = \frac{1 + B}{1 + 0.15 \mathrm{Re}_p^{0.687}} \frac{\rho_p D^2}{18 \mu} \tag{29}$$

Neglecting radial velocity fluctuations $v_p \simeq v_{p,0}$ [2, 57], Eq. (28) yields to the first order approximation:

$$\frac{\partial u_{p,1}}{\partial t} + u_{p,1} \frac{\partial u_{p,0}}{\partial x} + u_{p,0} \frac{\partial u_{p,1}}{\partial x} + v_p \frac{\partial u_{p,1}}{\partial r} = -\frac{\delta u_{p,1}}{\tau_{v,0}} + \frac{\delta u_{p,0}}{\tau_{v,0}^2} \tau_{v,1} \tag{30}$$

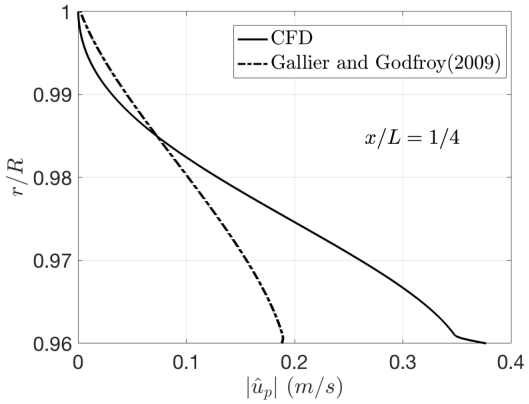

Fig. 7 Modulus of axial droplet velocity fluctuations $|\hat{u}_p|$ at $x/L = 1/4$ in the aluminum combustion zone. Solid line : CFD. Dashed dotted lines : Eq. (32)**.**

By further neglecting the advection terms and the fluctuating drag characteristic time in Eq. (30), it comes [27]:

$$\frac{\partial u_{p,1}}{\partial t} = -\frac{\delta u_{p,1}}{\tau_{v,0}} \tag{31}$$

In the Fourier space, Eq. (31) gives [16, 27]:

$$\hat{u}_p = \frac{\hat{u}}{1 + i\omega\tau_{v,0}} \tag{32}$$

Substituting Eq. (31) in Eq. (27), one finally obtains:

$$\frac{\hat{\dot{q}}}{\dot{q}_0} = -\frac{\mathrm{Sh}_0 - 2}{2\mathrm{Sh}_0} \frac{\omega\tau_{v,0}(i + \omega\tau_{v,0})}{1 + \omega^2\tau_{v,0}^2} \frac{\delta u_{p,0}}{|\delta \mathbf{u_p}|_0^2} \hat{u} \tag{33}$$

This transfer function gives the heat release rate fluctuations $\hat{\dot{q}}$ as a function of the mean flow properties and axial gas velocity fluctuations $\hat{u}$. The two expressions Eqs. (32) and (33) are compared to numerical flow simulations in Figs. 7 and 8, at the quarter of the motor chamber $x/L = 1/4$ and in the aluminum combustion zone. To be consistent, the mean flow properties in Eqs. (32) and (33) are taken from the simulation.

The modulus of the axial droplet velocity fluctuation $|\hat{u}_p|$ is plotted in Fig. 7. The analytical model Eq. (32), in which $\hat{u}$ and $\tau_{v,0}$ are taken from the simulation, reproduces roughly the behavior observed in the simulation close to the propellant surface at $r/R \sim 1$, but the results rapidly deviate as the distance to the propellant surface increases. This means that the low-pass filter Eq. (32) does not model correctly the axial droplet velocity fluctuations $\hat{u}_p$ in the aluminum combustion zone.

Figure 8 shows the modulus of the heat release rate fluctuations $|\hat{\dot{q}}|$ resulting from aluminum combustion. Numerical results from the flow solver are compared to the analytical expressions Eq. (33) from Gallier and Godfroy [23] and to predictions from Eq. (27), in which the axial gas velocity fluctuations $\hat{u}$ are taken in both cases from the flow solver. In

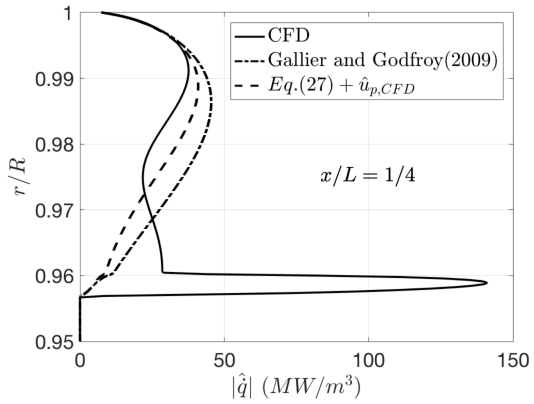

Fig. 8 Modulus of heat release rate fluctuations $|\hat{\dot{q}}|$ at $x/L = 1/4$ in the aluminum combustion zone. Solid line : CFD. Dashed dotted lines : Eq. (33)**. Dashed lines : Eq.** (27)**.**

Eq. (33), the droplet velocity fluctuations $\hat{u}_p$ are modeled with Eq. (32) and in Eq. (27) they are taken from the flow simulations.

The heat release rate fluctuations in Fig. 8 are not well reproduced by none of the models. Taking the correct gas $\hat{u}$ and particle $\hat{u}_p$ velocities improves the predictions with respect to the numerical flow simulation close to the propellant surface, but the heat release rate model Eq. (27) does not reproduce the correct trend over the entire combustion volume with important differences close to the boundary where droplet combustion is quenched. The numerical flow simulation highlights a high peak of heat release rate disturbances in Fig. 8 close to the end of the aluminum combustion zone. This peak results from the motion of the combustion volume boundary and is not reproduced by the analytical models. It has however been shown that this motion largely contributes to the thermo-acoustic source [24, 25].

In the following section, a new model is developed that better reproduces the heat release rate fluctuations inside the combustion volume and at the combustion volume boundary.

B. Heat release rate fluctuation model

The aluminum droplet lifetime is determined by the condition on the droplet diameter $D = D_r$ which is used to abruptly quench combustion with the Heaviside distribution in Eq. (13). It has been shown in [25] that droplet lifetime oscillations are likely to induce a fluctuating motion $\hat{r}_c$ of the boundary of the distributed combustion volume as in Fig. 3. This motion constitutes an additional source of heat release rate fluctuations and another thermo-acoustic source [24, 25] as illustrated in Fig. 5(b).

Heat release rate fluctuations observed at the boundary of the combustion zone and corresponding to the high peak in Fig. 8 originate from fluctuations of the Heaviside function and of the droplet diameter [25]. In Eqs. (13) and (18), neglecting droplet diameter fluctuations removes the impact of the Heaviside function and the source of heat release rate fluctuations due to droplet lifetime oscillations.

Considering a linear response of the heat release, fluctuations are decomposed as the sum of a volumetric contribution ($v.c.$) and a contribution ($b.c.$) from the boundary. Using this decomposition in Eq. (13) yields :

$$\hat{\dot{q}} = \hat{\dot{q}}_{v.c.} + \hat{\dot{q}}_{b.c.} = \hat{\dot{q}}_{D^2} \left(\mathcal{H}(D - D_r)\right)_0 + \dot{q}_{D^2,0} \widehat{\mathcal{H}(D - D_r)} \tag{34}$$

The boundary contribution can be expressed in the Fourier space as [25]:

$$\hat{\dot{q}}_{b.c.} = -\dot{q}_{D^2,0} \frac{2}{\pi} \left(1 - \left(\frac{r - r_{c,0}}{|\hat{r}_c|}\right)^2\right)^{1/2} \frac{\hat{r}_c}{|\hat{r}_c|} \tag{35}$$

where r is the radial position and $\hat{r}_c$ the Fourier component of the radial disturbance around the mean position $r_{c,0}$ of the boundary of the combustion zone. This model is restricted to radial fuel droplet trajectories, which is a reasonable approximation due to the small thickness of the combustion volume (see Fig. 3). This contribution results from local nonlinearities of the heat release rate at the end of the combustion process. The mean boundary position $r_{c,0}$ is given by [25]:

$$r_{c,0} = R + \frac{2}{D_i^2 - D_r^2} \int_{D_i}^{D_r} t_{c,0} v_p D_0 dD \tag{36}$$

with $t_{c,0}$ the mean droplet lifetime:

$$t_{c,0} = \frac{\rho_p \mathrm{Pr}(D_i^2 - D_r^2)}{4\mu \ln(1 + \mathrm{B})\mathrm{Sh}} \tag{37}$$

The motion of the combustion volume boundary is linked to droplet diameter fluctuations and to the mean flow by [25]:

$$\hat{r}_c = \frac{2 t_{c,0} v_p D_0}{D_i^2 - D_r^2} \hat{D} \tag{38}$$

Fluctuations of the droplet diameter drive droplet lifetime oscillations, but also change the dynamics at which heat is released in the combustion volume. Linearization of Eq. (11) for the mass flow rate $\dot{m}_{D^2}$ yields an expression for the volumetric contribution to heat release rate fluctuations:

$$\hat{\dot{q}}_{v.c} = \dot{q}_0 \left(\frac{\mathrm{Sh}_0 - 2}{2\mathrm{Sh}_0} \frac{\delta u_{p,0}}{|\delta \mathbf{u_p}|_0^2} (\hat{u}_p - \hat{u}) + \left(1 + \frac{\mathrm{Sh}_0 - 2}{2\mathrm{Sh}_0}\right) \frac{\hat{D}}{D_0}\right) \tag{39}$$

This expression is an extension of Eq. (27) by considering that the flow not only alters the droplet velocity, but also modifies the droplet diameter.

Summing the volumetric and boundary contributions to heat release rate disturbances yields:

$$\frac{\hat{\dot{q}}}{\dot{q}_0} = \frac{\mathrm{Sh}_0 - 2}{2\mathrm{Sh}_0} \frac{\delta u_{p,0}}{|\delta \mathbf{u_p}|_0^2} (\hat{u}_p - \hat{u}) + \left(1 + \frac{\mathrm{Sh}_0 - 2}{2\mathrm{Sh}_0}\right) \frac{\hat{D}}{D_0} - \frac{\dot{q}_{D^2,0}}{\dot{q}_0} \frac{2}{\pi} \left(1 - \left(\frac{r - r_{c,0}}{|\hat{r}_c|}\right)^2\right)^{1/2} \frac{\hat{r}_c}{|\hat{r}_c|} \tag{40}$$

Heat release rate fluctuations $\hat{\dot{q}}$ now depend on the mean flow properties, droplet velocity $\hat{u}_p$ and gas velocity $\hat{u}$ fluctuations and droplet diameter $\hat{D}$ fluctuations. These disturbances can be expressed as a function of the axial gas velocity disturbances $\hat{u}$ and the mean flow properties only. To close the model Eq. (40), it is necessary to express the droplet diameter $\hat{D}$ and droplet velocity $\hat{u}_p$ fluctuations as functions of the mean flow properties and gas velocity fluctuations $\hat{u}$.

The governing transport equations for droplet diameter and droplet axial velocity disturbances are derived as follows. In subsection IV.A, all the advection terms in Eq. (30) were neglected. However, as aluminum combustion takes place in the acoustic boundary layer (see Fig. 6), the radial gradients of the droplet velocity $\partial u_{p,1}/\partial r$ and gas velocity $\partial u_1/\partial r$ fluctuations cannot be neglected. This leads to a new transport equation for droplet velocity fluctuations which is a simplification of Eq. (30) by only retaining the radial advection term and the drag characteristic time fluctuations:

$$\frac{\partial u_{p,1}}{\partial t} + v_p \frac{\partial u_{p,1}}{\partial r} = -\frac{\delta u_{p,1}}{\tau_{v,0}} + \frac{\delta u_{p,0}}{\tau_{v,0}^2}\tau_{v,1} \tag{41}$$

A linearization of τ_v given by Eq. (29) yields:

$$\frac{\tau_{v,1}}{\tau_{v,0}} = (2 - C_{Re})\frac{D_1}{D_0} - C_{Re}\frac{\delta u_{p,0}}{|\delta \mathbf{u_{p,0}}|_0^2}(u_{p,1} - u_1) \tag{42}$$

in which C_{Re} depends on the mean particle Reynolds number $Re_{p,0}$ (Eq. (15)):

$$C_{Re} = \frac{0.10305 Re_{p,0}}{1 + 0.15 Re_{p,0}} \tag{43}$$

Combining the transport equations Eqs. (5)–(8) for the mass of the droplet phase $\alpha_p \rho_p$ and for the number N_p of particles per unit volume with the definition of the droplet diameter D given by Eq. (10) yields a transport equation for the droplet diameter in an Eulerian framework:

$$\frac{\partial D}{\partial t} + \mathbf{u_p} \cdot \nabla D = -\frac{2\mu \ln(1 + \mathrm{B})\mathrm{Sh}}{\mathrm{Pr}\rho_p D} \tag{44}$$

Assuming that *(i)* the thickness of the combustion zone remains small with quasi-1D droplet trajectories as in Fig. 3, *(ii)* the rate of droplet injection at the propellant surface is uniform along the axial direction, *(iii)* the acoustic mode is locked to the first longitudinal acoustic mode of the motor and *(iv)* the droplet diameter is regressing along its trajectory with $\partial D_1/\partial r \neq 0$, all the advection terms can be neglected except the radial term in the linearization of Eq. (44):

$$\frac{\partial D_1}{\partial t} + v_p \frac{\partial D_1}{\partial r} = -\frac{2\mu \ln(1 + \mathrm{B}_0)\mathrm{Sh}_0}{\mathrm{Pr}\rho_p D_0}\left(\frac{\mathrm{Sh}}{D}\right)_1 \tag{45}$$

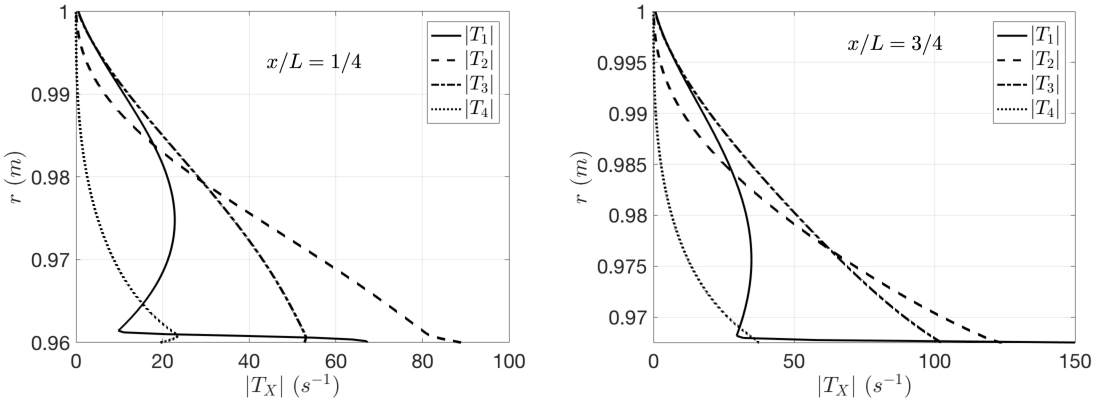

(a) $x/L = 1/4$ **(b)** $x/L = 3/4$

Fig. 9 Comparison between the modulus of the different terms from Eq. (49)**, at** $x/L = 1/4$ **and** $x/L = 3/4$ **in the SRM.**

with:

$$\left(\frac{\mathrm{Sh}}{D}\right)_1 = \frac{\mathrm{Sh}_0 - 2}{2\mathrm{Sh}_0}\frac{\delta u_{p,0}(u_{p,1} - u_1)}{|\delta u_p|_0^2} - \frac{\mathrm{Sh}_0 + 2}{2\mathrm{Sh}_0}\frac{D_1}{D_0} \tag{46}$$

The assumptions *(i)* to *(iv)* are realistic in many solid rocket motors. In the Fourier space, Eq. (41) yields a first order differential equation, in r, for $\hat{u}_p$:

$$\frac{\partial \hat{u}_p}{\partial r} + \frac{\hat{u}_p}{v_p \tau_{v,0}}\left(i\omega\tau_{v,0} + 1 + C_{Re}\frac{\delta u_{p,0}^2}{|\delta \mathbf{u_p}|_0^2}\right) = \frac{\hat{u}}{v_p \tau_{v,0}}\left(1 + C_{Re}\frac{\delta u_{p,0}^2}{|\delta \mathbf{u_p}|_0^2}\right) + \frac{\hat{D}\delta u_{p,0}}{D_0 v_p \tau_{v,0}}(2 - C_{Re}) \tag{47}$$

This equation depends on droplet diameter fluctuations $\hat{D}$ which are the solution of the Fourier transform of Eq. (45):

$$\frac{\partial \hat{D}}{\partial r} + \hat{D}\left(\frac{i\omega}{v_p} - \frac{\mu \ln(1+\mathrm{B})(\mathrm{Sh}_0 + 2)}{v_p \mathrm{Pr}\rho_p D_0^2}\right) = -\frac{\mu \ln(1+\mathrm{B})(\mathrm{Sh}_0 - 2)}{v_p \mathrm{Pr}\rho_p D_0 |\delta \mathbf{u_p}|_0^2 / \delta u_{p,0}}(\hat{u}_p - \hat{u}) \tag{48}$$

The expressions (47) and (48) constitute a system of two coupled ordinary differential equations for the droplet velocity and droplet diameter fluctuations. It has no straightforward analytical solution. It can be resolved numerically or further simplified in an attempt to find analytical solutions. To do so, a term in the equation system (47) and (48) needs to be removed. The most appropriate equation to reduce is Eq. (47):

$$\underbrace{\frac{\partial \hat{u}_p}{\partial r}}_{T_1} + \underbrace{\frac{\hat{u}_p}{v_p \tau_{v,0}}\left(i\omega\tau_{v,0} + 1 + C_{Re}\frac{\delta u_{p,0}^2}{|\delta \mathbf{u_p}|_0^2}\right)}_{T_2} = \underbrace{\frac{\hat{u}}{v_p \tau_{v,0}}\left(1 + C_{Re}\frac{\delta u_{p,0}^2}{|\delta \mathbf{u_p}|_0^2}\right)}_{T_3} + \underbrace{\frac{\hat{D}}{D_0}\frac{\delta u_{p,0}}{v_p \tau_{v,0}}(2 - C_{Re})}_{T_4} \tag{49}$$

where T_1, T_2, T_3 and T_4 designate the four terms in Eq. (49). The modulus of these terms calculated by direct numerical flow simulations are plotted in Fig. 9 in the combustion zone at $x/L = 1/4$ and $x/L = 3/4$, where the thermo-acoustic

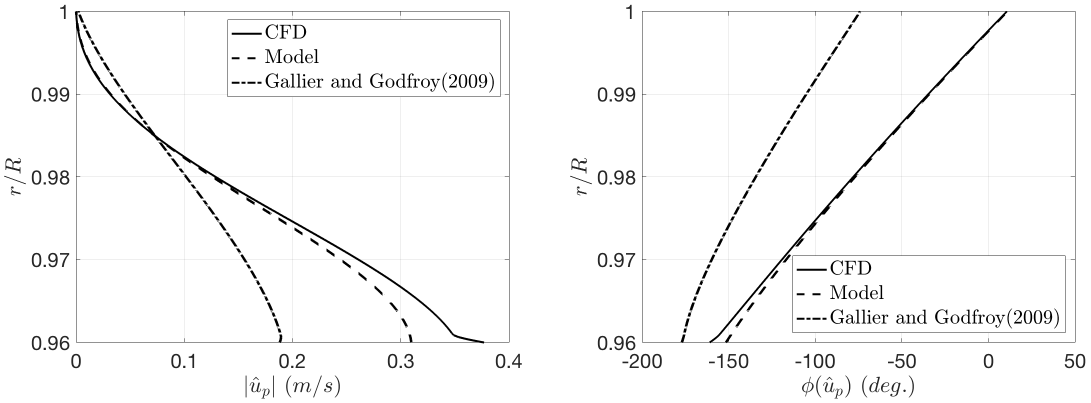

(a) Modulus **(b) Phase lag**

Fig. 10 Droplet velocity fluctuation $\hat{u}_p$ in the aluminum combustion zone at $x/L = 1/4$. Solid line : CFD. Dashed lines : Eq. (51). Dashed dotted lines : Eq. (33).

coupling is the highest (Fig. 5(b)). Figure 9 shows that the advection term T_1 cannot be neglected as expected and that T_4 associated to droplet diameter fluctuations is smaller than the other contributions. Neglecting T_4 leads to an analytical solution of the ordinary differential system Eqs. (47) and (48). In that case, Eq. (47) is reduced to:

$$\frac{\partial \hat{u}_p}{\partial r} + \frac{\hat{u}_p}{v_p \tau_{v,0}} \left(i\omega\tau_{v,0} + 1 + C_{Re} \frac{\delta u_{p,0}^2}{|\delta \mathbf{u_p}|_0^2} \right) = \frac{\hat{u}}{v_p \tau_{v,0}} \left(1 + C_{Re} \frac{\delta u_{p,0}^2}{|\delta \mathbf{u_p}|_0^2} \right) \tag{50}$$

This expression does not depend on $\hat{D}$. It is at this stage worth reminding that radial velocity, density and temperature fluctuations were neglected. The injected mass flow rate at the solid propellant boundary $r/R = 1$ is kept constant and axial velocity fluctuations are zero $\hat{u}(r = R) = 0$ at this boundary. As a consequence, droplet velocity and droplet diameter fluctuations at the injection boundary are therefore also equal to zero : $\hat{u}_p(r = R) = 0$, $\hat{D}(r = R) = 0$. The solution of Eq. (50) for $\hat{u}_p(r = R) = 0$ is:

$$\hat{u}_p = \int_R^r \frac{\hat{u}}{v_p \tau_{v,0}} \left(1 + C_{Re} \frac{\delta u_{p,0}^2}{|\delta \mathbf{u_p}|_0^2} \right) \exp\left(\int_r^{r'} \left(i\omega\tau_{v,0} + 1 + C_{Re} \frac{\delta u_{p,0}^2}{|\delta \mathbf{u_p}|_0^2} \right) \frac{dr''}{v_p \tau_{v,0}} \right) dr' \tag{51}$$

One now introduces the transfer function $\mathcal{F}_p = \hat{u}_p/\hat{u}$. This transfer function is linear and depends on the structure of the acoustic boundary layer and on the history of the fuel droplets during their transport, from their injection plane to their current radial position r. Equation (48) can now be resolved by substitution of the solution Eq. (51) for $\hat{D}(r = R) = 0$:

$$\hat{D} = -\int_R^r \hat{u} \frac{\mu \ln(1+\mathrm{B})(\mathrm{Sh}_0 - 2)}{v_p \mathrm{Pr} \rho_p D_0 |\delta \mathbf{u_p}|_0^2 / \delta u_{p,0}} (\mathcal{F}_p - 1) \exp\left(\int_r^{r'} \left(\frac{i\omega}{v_p} - \frac{\mu \ln(1+\mathrm{B})(\mathrm{Sh}_0 + 2)}{v_p \mathrm{Pr} \rho_p D_0^2} \right) dr'' \right) dr' \tag{52}$$

The expressions Eq. (51) for the droplet velocity fluctuations $\hat{u}_p$ and Eq. (52) for the droplet diameter fluctuations $\hat{D}$

can now be compared to numerical simulation results. The mean flow quantities and the gas velocity fluctuations $\hat{u}$ are again taken from the flow simulations to evaluate Eqs. (51) and (52).

The modulus and phase lag of the droplet velocity fluctuations $\hat{u}_p$ calculated with Eq. (51), with Eq. (32) from Gallier and Godfroy model and from direct numerical flow simulations are compared in Fig. 10 in the aluminum combustion zone at the quarter of the chamber $x/L = 1/4$. In all the following figures, the phase lag is expressed with respect to the acoustic pressure. The new model Eq. (51) fits better the numerical flow results than Eq. (32), justifying to consider the advection term in Eq. (50) due to the presence of the acoustic boundary layer and fluctuations of the drag characteristic time in response to gas and droplet velocity disturbances. A slight difference is observed between this new model and results from the numerical flow simulations at the end of the combustion zone for $0.96 \leq r/R \leq 0.98$ because the contribution T_4 in Eq. (49) from droplet diameter fluctuations have been neglected in the droplet velocity fluctuation model. The model Eq. (51) for $\hat{u}_p$ also yields a good match with the numerical flow simulations at the other axial positions in the SRM chamber.

Equation (52) yields a model for droplet diameter disturbances $\hat{D}$ in an acoustically forced flow. It is worth recalling that Eq. (52) depends on Eq. (51) for the droplet velocity fluctuations $\hat{u}_p$ due to the acoustic field. Equation (52) is compared to numerical flow results in Fig. 11 for the modulus and the phase lag at the quarter of the tube $x/L = 1/4$ in the aluminum combustion zone. One recalls that the phase lag is expressed with respect to the acoustic pressure. The model yields very close results to the numerical flow simulations over the entire volume of the combustion zone, even at the end of the combustion process. This proves the low impact of neglecting droplet diameter fluctuations in the droplet velocity fluctuation model by removing the term T_4 in Eq. (49). Close to the injection plane for $0.995 \leq r/R \leq 1$, the modeled phase lag does not fit well to CFD simulations, certainly because the radial velocity fluctuations have been neglected $v_p = v_{p,0}$ in Eq. (52). However, as the diameter modulus $|\hat{D}|$ is close to zero in this region, these differences do not alter the results. It was checked that the model Eq. (52) yields similar results at other axial positions in the SRM.

The new expression for the heat release rate fluctuations $\hat{\dot{q}}$ is recalled here:

$$\frac{\hat{\dot{q}}}{\dot{q}_0} = \frac{\mathrm{Sh}_0 - 2}{2\mathrm{Sh}_0} \frac{\delta u_{p,0}}{|\delta \mathbf{u_p}|_0^2} (\hat{u}_p - \hat{u}) + \left(1 + \frac{\mathrm{Sh}_0 - 2}{2\mathrm{Sh}_0}\right) \frac{\hat{D}}{D_0} - \frac{\dot{q}_{D^2,0}}{\dot{q}_0} \frac{2}{\pi} \left(1 - \left(\frac{r - r_{c,0}}{|\hat{r}_c|}\right)^2\right)^{1/2} \frac{\hat{r}_c}{|\hat{r}_c|} \tag{53}$$

$$\hat{r}_c = \frac{2t_{c,0} v_p D_0}{D_i^2 - D_r^2} \hat{D} \tag{54}$$

$$\hat{u}_p = \int_R^r \frac{\hat{u}}{v_p \tau_{v,0}} \left(1 + C_{Re} \frac{\delta u_{p,0}^2}{|\delta \mathbf{u_p}|_0^2}\right) \exp\left(\int_r^{r'} \left(i\omega\tau_{v,0} + 1 + C_{Re} \frac{\delta u_{p,0}^2}{|\delta \mathbf{u_p}|_0^2}\right) \frac{dr''}{v_p \tau_{v,0}}\right) dr' \tag{55}$$

$$\hat{D} = -\int_R^r \hat{u} \frac{\mu \ln(1 + \mathrm{B})(\mathrm{Sh}_0 - 2)}{v_p \mathrm{Pr} \rho_p D_0 |\delta \mathbf{u_p}|_0^2 / \delta u_{p,0}} (\mathcal{F}_p - 1) \exp\left(\int_r^{r'} \left(\frac{i\omega}{v_p} - \frac{\mu \ln(1 + \mathrm{B})(\mathrm{Sh}_0 + 2)}{v_p \mathrm{Pr} \rho_p D_0^2}\right) dr''\right) dr' \tag{56}$$

with $\mathcal{F}_p = \hat{u}_p / \hat{u}$. This model yields the heat release rate perturbations $\hat{\dot{q}}$ from the burning cloud of aluminum droplets

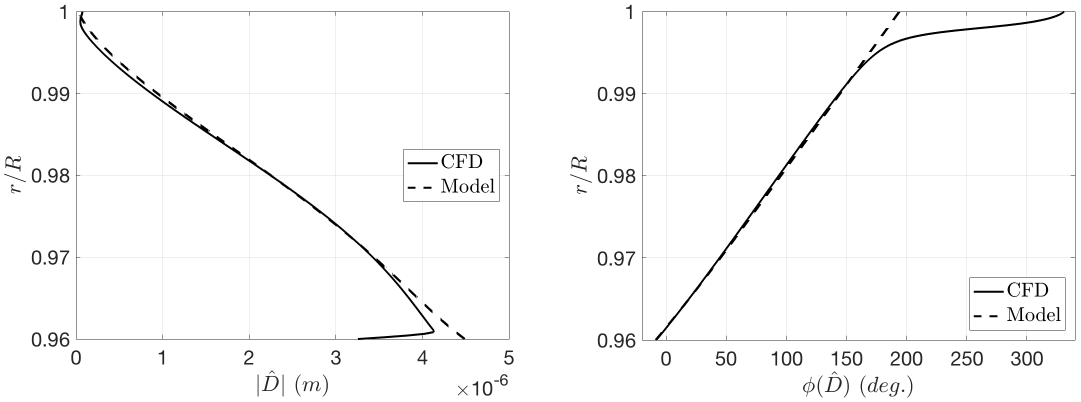

(a) Modulus **(b) Phase lag**

Fig. 11 Droplet diameter fluctuation $\hat{D}$ in the aluminum combustion zone at $x/L = 1/4$. Solid line : CFD. Dashed lines : Eq. (52)**.**

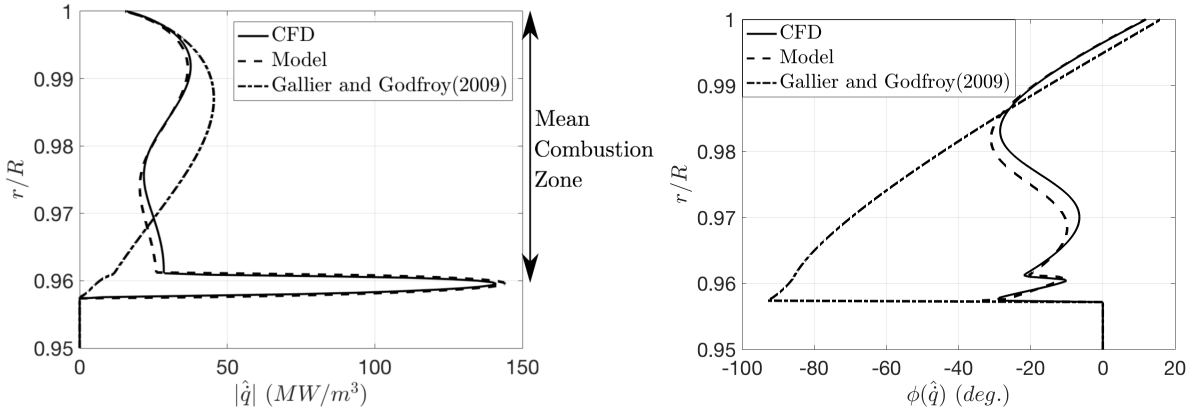

(a) Modulus **(b) Phase lag**

Fig. 12 Heat release rate fluctuations $\hat{\dot{q}}$ in the aluminum combustion zone at $x/L = 1/4$. Solid line : CFD. Dashed lines : Eq. (53)**. Dashed dotted lines : Eq.** (33)**.**

as a function of the mean flow properties and of the axial gas velocity fluctuations $\hat{u}$. To compare this model and the heat release rate fluctuations calculated by the numerical flow solver, the mean flow quantities and the axial gas velocity fluctuations $\hat{u}$ are extracted from the CFD simulations.

Figures 12 and 13 compare the modulus and phase lag of the heat release rate disturbances $\hat{\dot{q}}$ given by the new model, by the model from Gallier and Godfroy [23] and by the numerical flow simulation at two locations $x/L = 1/4$ and $x/L = 3/4$ in the aluminum combustion zone. These locations correspond to extrema of the local Rayleigh source term $\mathcal{S}$ shown in Fig. 5(b).

The new model is very close to numerical flow simulation results at both axial positions and better fits than the model from Gallier and Godfroy [23] in Figs. 12 and 13. In the combustion volume, no significant differences can be

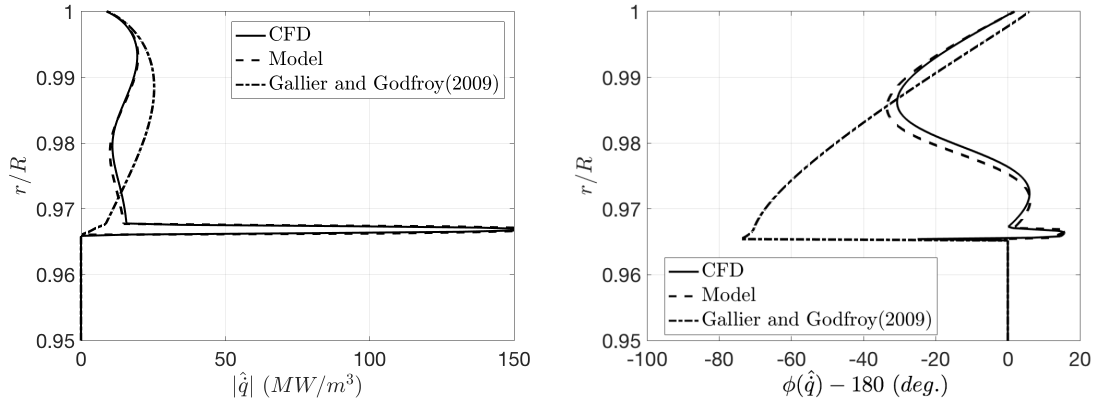

(a) Modulus **(b) Phase lag**

Fig. 13 Heat release rate fluctuations $\hat{\dot{q}}$ in the aluminum combustion zone at $x/L = 3/4$. Solid line : CFD. Dashed lines : Eq. (53). Dashed dotted lines : Eq. (33).

observed allowing to validate the assumption made on T_4 in Eq. (49) and the expression derived to model the volumetric contribution $\hat{\dot{q}}_{v.c.}$ to the heat release rate fluctuation. The boundary flapping motion $\hat{r}_c$ is also well reproduced and the heat release rate modulus and phase lag are also very close to the numerical flow results in this region. The heat release rate fluctuations in the flapping zone essentially depend on $\hat{\dot{q}}_{b.c.}$, which are directly linked to the modulus of the flapping motion $|\hat{r}_c|$ and to the pressure amplitude $\hat{\eta}$ pulsation [25]. In the expression for $\hat{\dot{q}}_{b.c.}$, the flapping motion has been assumed to be symmetrical with respect to its mean position and comparisons with numerical flow simulations allow to validate this assumption in the linear regime.

Agreement between the new model and direct numerical flow simulations has been checked at other axial positions through the motor. The slight differences which can be observed between the model and the simulation results in Figs. 12 and 13 are due to the different approximations made by neglecting T_4 and assuming $\hat{v} = 0$, $\hat{v}_p = 0$, $\hat{T}_g = 0$, $\hat{\rho}_g = 0$, $\hat{N}_p = 0$ and $\partial/\partial x = 0$ to get the analytical results.

C. Axial gas velocity model within the aluminum combustion zone

In the previous section, heat release rate fluctuations $\hat{\dot{q}}$ were derived as a function of the mean flow properties and of axial gas velocity fluctuations $\hat{u}$. These latter quantities were both extracted from numerical flow simulations. To get a full analytical model for $\hat{\dot{q}}$ which does not require to conduct an unsteady two-phase flow simulation, a model for the axial velocity fluctuations $\hat{u}$ taking place in the aluminum combustion is needed.

Flandro *et al.* [57] derived an expression for this velocity in the acoustic boundary layer of an isentropic flow. In this model, the perturbed velocity is split into an acoustic and rotational part:

$$\hat{u} = \hat{u}_{ac} + \hat{u}_{rot} \tag{57}$$

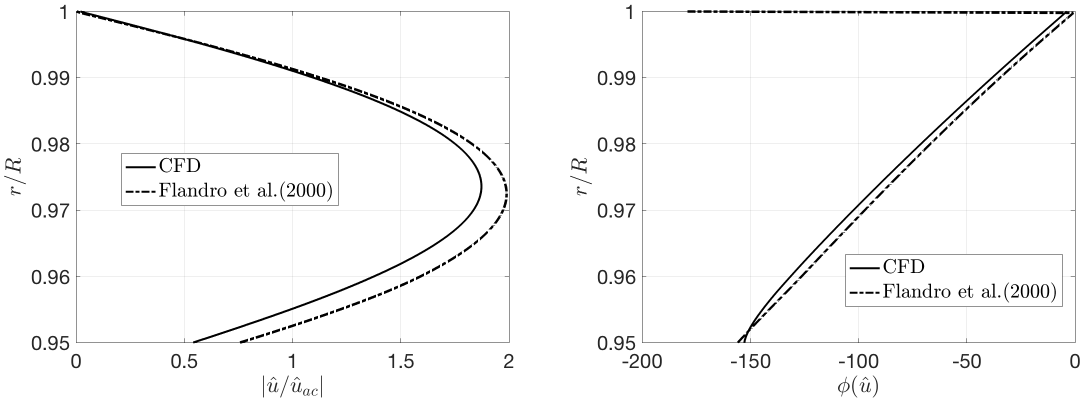

(a) Modulus **(b) Phase lag**

Fig. 14 Axial gas velocity fluctuations $\hat{u}$ in the aluminum combustion zone at $x/L = 1/4$. Solid line : CFD. Dashed dotted lines : Eq. (57).

where the acoustic component is assumed to correspond to the first longitudinal mode of a closed-closed chamber cavity:

$$\hat{u}_{ac} = -\frac{i\hat{\eta}}{a_0\rho}\sin(kx) \quad \text{where} \quad k = \frac{\omega}{a_0} \tag{58}$$

with a_0 the speed of sound, $\rho = \alpha_p\rho_p + \rho_g$ the density of a two-phase flow and $\hat{\eta}$ the pressure amplitude. The rotational contribution in Eq. (57) is given by:

$$\hat{u}_{rot} = -\frac{i\hat{\eta}}{a_0\rho}\left[\beta\frac{r}{R}\sin(kx\sin\Theta)\exp\left(\Phi + i\frac{S_r}{\pi}\ln\left(\tan\frac{\Theta}{2}\right)\right)\right] \tag{59}$$

with Φ a complex expression given in [57], $\Theta = \frac{\pi}{2}(r/R)^2$ and β is equal to:

$$\beta = \frac{C_\beta}{S_r}\left(\frac{r}{R}\sin\Theta + i\frac{\xi R}{S_r r\sin\Theta}\right) \tag{60}$$

where R is the chamber radius, S_r the Strouhal number, ξ a viscous parameter and C_β a constant of integration. These quantities are given in [57]:

$$S_r = \frac{\omega R}{v_i} \quad \xi = \frac{S_r^2}{Re_i} \quad C_\beta = -\frac{S_r^3\left(\left(S_r^2+\xi\right) - iS_r\xi\right)}{\left(S_r^2+\xi\right)^2 + (S_r\xi)^2} \tag{61}$$

with v_i the (radial) gas injection velocity and $Re_i = (\rho v_i R)/\mu$ the injection Reynolds number, ρ the mixture density and μ the dynamic viscosity.

Radial profiles of the modulus and phase lag of the axial gas velocity $\hat{u}$ calculated with Eq. (57) in the aluminum combustion zone at $x/L = 1/4$ are plotted in Fig. 14. Results are compared with direct numerical flow simulations. In this figure, the phase lag is again expressed with respect to the acoustic pressure and the modulus is normalized by the

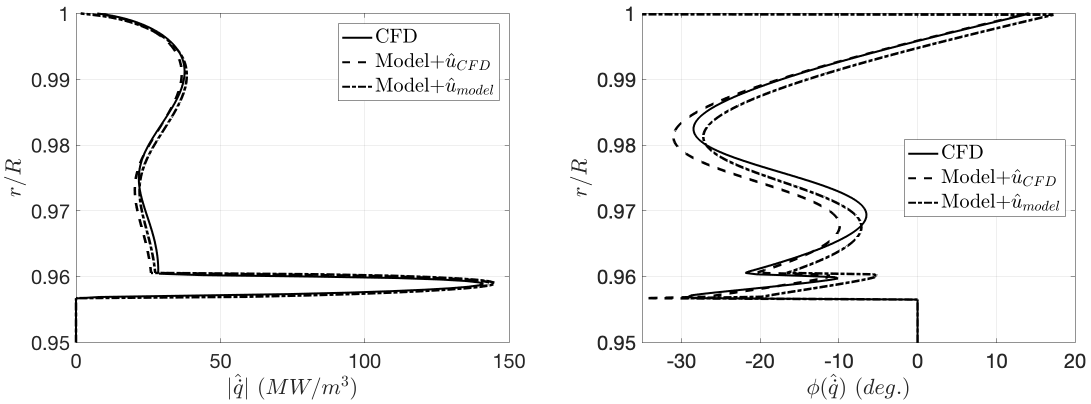

(a) Modulus **(b) Phase lag**

Fig. 15 Heat release rate fluctuations $\hat{\dot{q}}$ in the aluminum combustion zone at $x/L = 1/4$. Solid line : CFD. Dashed lines : Eq. (53) with $\hat{u}$ from CFD. Dashed dotted lines : Eq. (53) with $\hat{u}$ given by Eq. (57).

acoustic velocity fluctuations $\hat{u}_{ac}$ which is invariant in the radial direction. Slight differences can be observed for the modulus of the axial velocity fluctuation $\hat{u}$ between this model and numerical flow results due to deviations of the real flow from a perfectly isentropic flow and single phase flow as assumed in the analytical model. For the phase lag, direct flow simulations and analytical results are very close. These comparisons yield similar results at all axial locations in the SRM. One may then safely conclude that the entropic contribution associated to the heat release rate to the velocity fluctuations $\hat{u}$ can be neglected in the SRM.

A final comparison is made by analyzing the impact of this model in the estimates of the heat release rate fluctuations. Results for the heat release rate fluctuations $\hat{\dot{q}}$ given by the numerical flow solver are compared in Fig. 15 to the model Eq. (53) with the velocity fluctuations $\hat{u}$ extracted from the numerical flow simulations and with the velocity fluctuations $\hat{u}$ modeled by Eq. (57) at the quarter of the tube $x/L = 1/4$, in the aluminum combustion zone. In the latter case, the heat release rate fluctuations are deduced from the knowledge of the mean flow properties, the forcing angular frequency ω and the pressure amplitude $\hat{\eta}$. Results with this fully analytical model are found to be very close to the other results in Fig. 15. The same observations can be made at other axial positions within the SRM.

These comparisons indicate that small heat release rate disturbances $\hat{\dot{q}}$ are well predicted by the analytical model developed in this work provided the mean flow properties and the modal structure of the acoustic mode are known through the SRM. This model may in turn be used to conduct a linear stability analysis for different operating conditions of the SRM as illustrated in the Appendix. This model may also be compared to experimental data from T-burners showing aluminum combustion driven instabilities [22].

V. Conclusion

The way acoustic perturbations lead to heat release rate disturbances originating from aluminum droplet combustion has been investigated numerically and theoretically in a generic SRM.

Numerical flow simulations have been used to analyze the origin of thermo-acoustic instabilities driven by the combustion dynamics of aluminum droplets by carefully avoiding other coupling mechanisms linked to hydrodynamic instabilities in a laminar flow configuration. These simulations are based on an Eulerian framework, for the gaseous and disperse phases, in which the combustion of disperse droplets is modeled by the D^2 law which is abruptly quenched when the droplet diameter falls below a threshold level to model the formation of aluminum oxide residues.

Analysis of the heat release rate and the Rayleigh source term distributions through the motor chamber has revealed two contributions to acoustic pressure oscillations. The first one corresponds to heat release rate fluctuations produced within the volume of the reactive droplet cloud. The second source of heat release rate disturbances originates from the flapping boundary of the droplet cloud. The volumetric contribution to heat release rate fluctuations results from the individual response of each aluminum droplet to the unsteady flow which is synchronized by the acoustic forcing. This flow produces an unsteady drag on each droplet and alters the droplet velocity and droplet diameter leading in turn to disturbances of the droplet fuel consumption rate. The second contribution is due to oscillations of the droplet lifetime induced by the history of the droplet dynamics in the acoustically perturbed flow. These fluctuations lead in turn to a motion of the boundary of the combustion volume resulting in large heat release rate fluctuations. This boundary contribution is very sensitive to the heat release rate value just before the droplet extinction. Modeling the end of aluminum droplet combustion requires further effort and has been here assumed to be reproduced by an Heaviside step function with abrupt quench of combustion when the droplet diameter falls below a threshold value.

Analytical models have been derived for these two contributions to heat release rate fluctuations and have been compared to numerical flow results. These models take into account both droplet diameter fluctuations and droplet velocity fluctuations in response to the acoustic forcing. They are used to determine the heat release rate disturbances originating from the droplet dynamics within the burning droplet cloud and the heat release rate disturbances originating from the motion of the burning droplet cloud boundary.

Different levels of approximations have been made to get an hybrid solution combining numerical and analytical results. A fully analytical model has also been derived in which the structure of the mean flow and the modal structure of the acoustic mode are the only inputs. This model has been shown to yield reliable estimates of the distribution and level of heat release rate fluctuations through the SRM in the limit of small acoustic disturbances. These models well reproduce the dynamics observed in the numerical flow simulations.

This heat release rate fluctuation model is well suited to conduct a linear stability analysis of the system dynamics and may be used to ease the prediction of thermo-acoustic instabilities in solid rocket motors or T-burners driven by aluminum droplet combustion. It also shed light on these dynamical phenomena without requiring intensive numerical

unsteady two-phase flow simulations.

Appendix : Linear stability analsis

The objective of this appendix is to illustrate how aluminum combustion contributes to instability growth rate and frequency shift in a SRM. Culick's [2, 6] time-space decomposition is used for pressure fluctuations :

$$p_1 = \hat{p}(\mathbf{x}) \exp(i\omega t) \quad \text{with} \quad \hat{p} = \sum_{n=1}^{\infty} \hat{\eta}_n \psi_n(\mathbf{x}) \tag{62}$$

The component $\hat{\eta}_n$ is the n$^{\text{th}}$-modal amplitude of the acoustic pressure fluctuation and ψ_n is the corresponding unperturbed acoustic mode which is solution of the Helmholtz equation. In the simulation, the modal distribution in the SRM is close to the unperturbed acoustic mode of an acoustically closed cavity at the two boundaries and is invariant in the radial direction [23]. No rotational or entropic effects are observed in the pressure distribution:

$$\psi_n = \cos(k_n x) \quad \text{and} \quad k_n = \frac{\omega_n}{a_0} \tag{63}$$

The pressure modes are orthogonal. A linear stability analysis yields for each mode the instability growth rate α and an angular frequency shift $\delta\omega$ from the unperturbed state [2, 6] :

$$\alpha_n = \alpha_{n,Al} + \alpha_{n,l} \quad \text{and} \quad \delta\omega_n = \delta\omega_{n,Al} + \delta\omega_{n,l} \tag{64}$$

where the subscript Al stands for sound sources associated the unsteady aluminum combustion and the subscript l stands for the other sound contributions that mainly correspond to acoustic losses. These losses are due to acoustic attenuation due to flow turning and interaction with inert droplets, convection and radiation of acoustic waves through the nozzle and the solid propellant impedance [2, 6].

The aluminum combustion contribution to instability growth rate is expressed as [6, 23]:

$$\alpha_{n,Al} = \frac{(\gamma - 1)}{E_n^2} \int_V \psi_n \mathcal{R}e\left(\frac{\hat{\dot{q}}}{\hat{\eta}_n}\right) dV \tag{65}$$

where $\mathcal{R}e$ stands for the real part, V the chamber volume and E_n^2 the acoustic energy of mode n:

$$E_n^2 = \int_V \psi_n^2 dV \tag{66}$$

For the cylindrical motor studied in this work one has $dV = r dr d\theta dx$. The corresponding frequency shift induced by

unsteady aluminum combustion is [6]:

$$\delta\omega_{n,Al} = \frac{(\gamma-1)}{E_n^2}\int_V \psi_n \mathcal{I}m\left(\frac{\hat{\dot{q}}}{\hat{\eta}_n}\right)dV \tag{67}$$

with $\mathcal{I}m$ the imaginary part.

Two contributions to heat release disturbances have been identified in this work: a volumetric contribution $v.c.$ due to the individual response of each droplet and a boundary contribution $b.c.$ due to droplet lifetime oscillations. The growth rate and the frequency shift associated to each of these contributions can be identically split as :

$$\alpha_{n,Al} = \alpha_{n,v.c} + \alpha_{n,b.c} \quad \text{and} \quad \delta\omega_{n,Al} = \delta\omega_{n,v.c} + \delta\omega_{n,b.c} \tag{68}$$

The volumetric contribution for the growth rate and the frequency shift can be written as:

$$\alpha_{n,v.c.} = \frac{2(\gamma-1)}{R^2\int_0^L \psi_n^2 dx}\int_0^L \psi_n \int_0^R \mathcal{R}e\left(\frac{\hat{\dot{q}}_{v.c.}}{\hat{\eta}_n}\right) r dr dx \tag{69}$$

$$\delta\omega_{n,v.c.} = \frac{2(\gamma-1)}{R^2\int_0^L \psi_n^2 dx}\int_0^L \psi_n \int_0^R \mathcal{I}m\left(\frac{\hat{\dot{q}}_{v.c.}}{\hat{\eta}_n}\right) r dr dx \tag{70}$$

in which $\hat{\dot{q}}_{v.c.}$ can be substituted by Eqs. (39), (52) and (51). This operation yields the expressions for $\alpha_{n,v.c.}$ and $\delta\omega_{n,v.c.}$ that only depend on the structure of the mean flow in the SRM, the structure of the acoustic boundary layer and the acoustic mode. In the linear regime, these expressions do not depend on the pressure amplitude.

For the boundary contribution, the expression for $\hat{\dot{q}}_{b.c.}$ now depends on the amplitude of the boundary motion $|\hat{r}_c|$ as given by Eq. (35). This causes a small difficulty in estimating the instability growth rate in the linear regime. One can proceed as follows to solve this issue. The instability growth rate is *a priori* given by :

$$\alpha_{n,b.c.} = \frac{2(\gamma-1)}{R^2\int_0^L \psi_n^2 dx}\int_0^L \psi_n \int_0^R \mathcal{R}e\left(\frac{\hat{\dot{q}}_{b.c.}}{\hat{\eta}_n}\right) r dr dx \tag{71}$$

By substituting $\hat{\dot{q}}_{b.c.}$ with Eq. (35), one obtains :

$$\alpha_{n,b.c.} = \frac{-2(\gamma-1)}{R^2\int_0^L \psi_n^2 dx}\int_0^L \psi_n \int_0^R \frac{2}{\pi}\dot{q}_{D^2,0}\left(1-\left(\frac{r-r_{c,0}}{|\hat{r}_c|}\right)^2\right)^{1/2} \mathcal{R}e\left(\frac{\hat{r}_c}{|\hat{r}_c|\hat{\eta}_n}\right) r dr dx \tag{72}$$

One sees that $\alpha_{n,b.c.}$ depends on the amplitude $|\hat{r}_c|$ of the perturbation $\hat{r}_c$, but the flapping boundary zone is located between $r \in [r_{c,0} - |\hat{r}_c|, r_{c,0} + |\hat{r}_c|]$ in the radial direction. As this zone is thin (linear fluctuations) in comparison with the combustion thickness, $\dot{q}_{D^2,0}\mathcal{R}e\,(\hat{r}_c/(|\hat{r}_c|\hat{\eta}_n))$ is assumed invariant in r and taken at $r = r_{c,0}$ in the flapping boundary

zone. With this assumption, one has :

$$\frac{2}{\pi|\hat{r}_c|}\int_{r_{c,0}-|\hat{r}_c|}^{r_{c,0}+|\hat{r}_c|}\left(1-\left(\frac{r-r_{c,0}}{|\hat{r}_c|}\right)^2\right)^{1/2} rdr = r_{c,0} \tag{73}$$

Equation (72) reduces in this case to :

$$\alpha_{n,b.c.} = \frac{-2(\gamma-1)}{R^2\int_0^L \psi_n^2 dx}\int_0^L \dot{q}_{D^2,0}\psi_n r_{c,0}\mathcal{R}e\left(\frac{\hat{r}_c}{\hat{\eta}_n}\right)dx \tag{74}$$

The same method can be used to determine the corresponding angular frequency shift. The general expression *a priori* writes :

$$\delta\omega_{n,b.c.} = \frac{-2(\gamma-1)}{R^2\int_0^L \psi_n^2 dx}\int_0^L \psi_n\int_0^R \dot{q}_{D^2,0}\frac{2}{\pi}\left(1-\left(\frac{r-r_{c,0}}{|\hat{r}_c|}\right)^2\right)^{1/2}\mathcal{I}m\left(\frac{\hat{r}_c}{|\hat{r}_c|\hat{\eta}_n}\right)rdrdx \tag{75}$$

With the same approximation, this expression reduces to:

$$\delta\omega_{n,b.c.} = \frac{-2(\gamma-1)}{R^2\int_0^L \psi_n^2 dx}\int_0^L \dot{q}_{D^2,0}\psi_n r_{c,0}\mathcal{I}m\left(\frac{\hat{r}_c}{\hat{\eta}_n}\right)dx \tag{76}$$

The motion of the boundary $\hat{r}_c$ given by Eq. (38) is linear. The expressions Eqs. (74) and (76) yield an instability growth rate and a frequency shift associated to the boundary contribution to heat release rate fluctuations which do not depend on the acoustic pressure amplitude. They can be determined once the structures of the mean flow, the acoustic boundary layer and acoustic mode are set.

Combining $\alpha_{n,b.c.}$ and $\alpha_{n,v.c.}$ yields the growth rates of acoustic modes interacting with the combustion dynamics of aluminum droplets.

Acknowledgments

This work is cofunded by the French space agency Centre National d'Etudes Spatiales (CNES) and ArianeGroup. The authors would like to thank Julien Pichillou and Nathalie Cesco from CNES for their support.

References

[1] Price, E. W., "Solid Rocket Combustion Instability–An American Historical Account," *Nonsteady Burning and Combustion Stability of Solid Propellants*, edited by L. De Luca, E. W. Price, and M. Summerfield, Vol. 143, Chapter 1, Progress in Astronautics and Aeronautics, AIAA Washington, DC, 1992, pp. 1–16.

[2] Culick, F., "Unsteady Motions in Combustion Chambers for Propulsion Systems," AGARDograph, NATO/RTO-AG-AVT-039, 2006.

[3] Fabignon, Y., Dupays, J., Avalon, G., Vuillot, F., Lupoglazoff, N., Casalis, G., and Prévost, M., "Instabilities and Pressure

Oscillations in Solid Rocket Motors," *Aerospace Science and Technology*, Vol. 7, No. 3, 2003, pp. 191–200, doi: 10.1016/S1270-9638(02)01194-X.

[4] Blomshield, F., "Historical Perspective Of Combustion Instability In Motors-Case Studies," AIAA Paper 2001-3875, July 2001, doi: 10.2514/6.2001-3875.

[5] Anthoine, J., "Solid Propellant Pressure Oscillations," *VKI / STO-AVT-206 Lecture Series on Fluid Dynamics Associated to Launcher Developers, von Kármán Inst., Rhode-Saint-Genèse, Belgium*, April 2013.

[6] Culick, F. E. C. and Yang, V., "Prediction of the Stability of Unsteady Motions in Solid Propellant Rocket Motors," *Nonsteady Burning and Combustion Stability of Solid Propellants*, edited by L. De Luca, E. W. Price, and M. Summerfield, Vol. 143, Chapter 18, Progress in Astronautics and Aeronautics, AIAA Washington, DC, 1992, pp. 719–779.

[7] Gallier, S., Prevost, M., Hijlkema, J., and Roumy, M., "Effects of Cavity on Thrust Oscillations in Subscale Solid Rocket Motors," AIAA Paper 2009-5253, August 2009, doi: 10.2514/6.2009-5253.

[8] Hirschberg, L., Schuller, T., Collinet, J., Schram, C., and Hirschberg, A., "Analytical Model for the Prediction of Pulsations in a Cold-Gas Scale-Model of a Solid Rocket Motor," *Journal of Sound and Vibration*, Vol. 419C, 2018, pp. 452–468, doi: 10.1016/j.jsv.2018.01.025.

[9] Anthoine, J., Buchlin, J. M., and Hirschberg, A., "Effect of Nozzle Cavity on Resonance in Large SRM: Theoretical Modeling," *Journal of Propulsion and Power*, Vol. 18, No. 2, 2002, pp. 304–311, doi: 10.2514/2.5935.

[10] Hirschberg, L., Schuller, T., Schram, C., Collinet, J., Yiao, M., and Hirschberg, A., "Interaction of a Vortex with a Contraction in a 2-Dimensional Channel: Incompressible Flow Prediction of Sound Pulse," AIAA Paper 2017-3701, June 2017, doi: 10.2514/6.2017-3701.

[11] Brown, R. S., Dunlap, R., Young, S. W., and Waugh, R. C., "Vortex Shedding as a Source of Acoustic Energy in Segmented Solid Rockets," *Journal of Spacecraft and Rockets*, Vol. 18, No. 4, 1981, pp. 312–319, doi: 10.2514/3.57822.

[12] Vuillot, F., "Vortex-Shedding Phenomena in Solid Rocket Motors," *Journal of Propulsion and Power*, Vol. 11, No. 4, 1995, pp. 626–639, doi: 10.2514/3.23888.

[13] Fabignon, Y., Trubert, J. F., Lambert, D., Orlandi, O., and Dupays, J., "Combustion of Aluminum Particles in Solid Rocket Motors," AIAA Paper 2003-4807, July 2003, doi: 10.2514/6.2003-4807.

[14] Babuk, V. A., Vasilyev, V. A., and Malakhov, M. S., "Condensed Combustion Products at the Burning Surface of Aluminized Solid Propellant," *Journal of Propulsion and Power*, Vol. 15, No. 6, 1999, pp. 783–793, doi: 10.2514/2.5497.

[15] Devillers, R. W., Le Besnerais, G., Nugue, M., and Cesco, N., "Experimental Analysis of Solid-Propellant Surface during Combustion with Shadowgraphy Images: New Tools to Assist Aluminum-Agglomeration Modelling," *7th European Conference for Aeronautics and Space Sciences, Milan (Italy)*, EUCASS Paper 2017-327, July 2017, doi: 10.13009/EUCASS2017-327.

[16] Temkin, S. and Dobbins, R. A., "Attenuation and Dispersion of Sound by Particulate-Relaxation Processes," *The Journal of the Acoustical Society of America*, Vol. 40, No. 2, 1966, pp. 317–324, doi: 10.1121/1.1910073.

[17] Karnesky, A. L. and Colucci, S. E., "Recent Occurrences of Combustion Instability in Solid Rocket Motors-An overview," *Journal of Spacecraft and Rockets*, Vol. 12, No. 1, 1975, pp. 33–38, doi: 10.2514/3.56948.

[18] Brooks, K. P. and Beckstead, M. W., "Dynamics of Aluminum Combustion," *Journal of Propulsion and Power*, Vol. 11, No. 4, 1995, pp. 769–780, doi: 10.2514/3.23902.

[19] Beckstead, M. W., "A Summary of Aluminum Combustion," VKI Special Course on "Internal Aerodynamics in Solid Rocket Propulsion". Report Number RTO-EN-023, von Kármán Inst., Rhode-Saint-Genèse, Belgium, May 2002.

[20] Raun, R. L. and Beckstead, M. W., "A Numerical Model for Temperature Gradient and Particle Effects on Rijke Burner Oscillations," *Combustion and Flame*, Vol. 94, No. 1-2, 1993, pp. 1–24, doi: 10.1016/0010-2180(93)90015-U.

[21] Beckstead, M. and Butcher, A., "The Velocity Coupled T-Burner," AIAA Paper 1974-200, Jan-Feb 1974, doi: 10.2514/6.1974-200.

[22] Gallier, S., Briquet, B., and Yiao, M., "Aluminum Combustion Can Drive Instabilities in Solid Rocket Motors: T-Burner Study," *Journal of Propulsion and Power*, Vol. 35, No. 1, 2019, pp. 159–172, doi: 10.2514/1.B37034.

[23] Gallier, S. and Godfroy, F., "Aluminum Combustion Driven Instabilities in Solid Rocket Motors," *Journal of Propulsion and Power*, Vol. 25, No. 2, 2009, pp. 509–521, doi: 10.2514/1.37664.

[24] Genot, A., Gallier, S., and Schuller, T., "A Numerical Analysis of the Aluminium Combustion Driven Instability in Solid Rocket Motors," *7th European Conference for Aeronautics and Space Sciences, Milan (Italy)*, EUCASS Paper 2017-064, July 2017, doi: 10.13009/EUCASS2017-064.

[25] Genot, A., Gallier, S., and Schuller, T., "Thermo-Acoustic Instabilities Driven by Fuel Droplet Lifetime Oscillations," *Proceedings of the Combustion Institute*, Vol. 37, No. 4, 2019, pp. 5359–5366,
doi: 10.1016/j.proci.2018.05.108.

[26] Gallier, S., Sibe, F., and Orlandi, O., "Combustion Response of an Aluminum Droplet Burning in Air," *Proceedings of the Combustion Institute*, Vol. 33, No. 2, 2011, pp. 1949–1956,
doi: 10.1016/j.proci.2010.05.046.

[27] Dupays, J. and Vuillot, F., "Propagation of an Acoustic Wave in a Two-Phase Reactive Medium," AIAA Paper 1988-3696, July 1998,
doi: 10.2514/6.1998-3696.

[28] Priem, R. J. and Guentert, D. C., *Combustion Instability Limits Determined by a Nonlinear Theory and a One-Dimensional Model*, NASA TN D-1409, Washington, D.C, October 1962.

[29] Zhu, M., Dowling, A., and Bray, K., "Forced Oscillations in Combustors with Spray Atomizers," *Journal of Engineering for Gas Turbines and Power*, Vol. 124, No. 1, 2002, pp. 20–30,
doi: 10.1115/1.1396841.

[30] Eckstein, J., Freitag, E., Hirsch, C., Sattelmayer, T., Von der Bank, R., and Schilling, T., "Forced Low-Frequency Spray Characteristics of a Generic Airblast Swirl Diffusion Burner," *Journal of Engineering for Gas Turbines and Power*, Vol. 127(2), 2005, pp. 301–306,
doi: 10.1115/1.1789515.

[31] Giuliani, F., Gajan, P., Diers, O., and Ledoux, M., "Influence of Pulsed Entries on a Spray Generated by an Air-Blast Injection Device: An Experimental Analysis on Combustion Instability Processes in Aeroengines," *Proceedings of the Combustion Institute*, Vol. 29, No. 1, 2002, pp. 91–98,
doi: 10.1016/S1540-7489(02)80016-5.

[32] Carvalho, J. A., McQuay, M. Q., and Gotac, P. R., "The Interaction of Liquid Reacting Droplets with the Pulsating Flow in a Rijke-Tube Combustor," *Combustion and Flame*, Vol. 108, No. 1-2, 1997, pp. 87–103,
doi: 10.1016/S0010-2180(96)00106-X.

[33] Sujith, R. I., "An Experimental Investigation of Interaction of Sprays With Acoustic Fields," *Experiments in Fluids*, Vol. 38, No. 5, 2005, pp. 576–587,
doi: 10.1007/s00348-004-0912-1.

[34] Bind, V. K., Roy, S., and Rajagopal, C., "A Reaction Engineering Approach to Modeling Dust Explosions," *Chemical Engineering Journal*, Vol. 207, 2012, pp. 625–634,
doi: 10.1016/j.cej.2012.07.026.

[35] Chiu, H. H. and Liu, T. M., "Group Combustion of Liquid Droplets," *Combustion Science and Technology*, Vol. 17, No. 3-4, 1977, pp. 127–142,
doi: 10.1080/00102207708946823.

[36] Chiu, H. H., Kim, H. Y., and Croke, E. J., "Internal Group Combustion of Liquid Droplets," *Symposium (international) on combustion*, Vol. 19, No. 1, 1982, pp. 971–980,
doi: 10.1016/S0082-0784(82)80273-7.

[37] Nakamura, M., Akamatsu, F., Kurose, R., and Katsuki, M., "Combustion Mechanism of Liquid Fuel Spray in a Gaseous Flame," *Physics of Fluids*, Vol. 17, No. 12, 2005, pp. 123301,
doi: 10.1063/1.2140294.

[38] Kitano, T., Nishio, J., Kurose, R., and Komori, S., "Effects of Ambient Pressure, Gas Temperature and Combustion Reaction on Droplet Evaporation," *Combustion and Flame*, Vol. 161, No. 2, 2014, pp. 551–564,
doi: 10.1016/j.combustflame.2013.09.009.

[39] Annamalai, K., Ryan, W., and Dhanapalan, S., "Interactive Processes in Gasification and Combustion–Part III: Coal/Char Particle Arrays, Streams and Clouds," *Progress in Energy and Combustion Science*, Vol. 20, No. 6, 1994, pp. 487–618,
doi: 10.1016/0360-1285(94)90002-7.

[40] Kerstein, A. R. and Law, C. K., "Percolation in Combusting Sprays I: Transition from Cluster Combustion to Percolate Combustion in Non-Premixed Sprays," *Symposium (International) on Combustion*, Vol. 19, No. 1, 1982, pp. 961–969,
doi: 10.1016/S0082-0784(82)80272-5.

[41] Bucher, P., Yetter, R. A., Dryer, F. L., Parr, T. P., and Hanson-Parr, D., "PLIF Species and Ratiometric Temperature Measurements of Aluminum Particle Combustion in O2, CO2 and N2O Oxidizers, and Comparison with Model Calculations," *Symposium (International) on Combustion*, Vol. 27, No. 2, 1998, pp. 2421–2429,
doi: 10.1016/S0082-0784(98)80094-5.

[42] Bucher, P., Yetter, R. A., Dryer, F. L., Parr, T. P., Hanson-Parr, D. M., and Viceni, E. P., "Flames Structure Measurement of Single, Isolated Aluminum Particles Burning in Air," *Symposium (International) on Combustion*, Vol. 26, No. 2, 1996, pp. 1899–1908,
doi: 10.1016/S0082-0784(96)80012-9.

[43] Duterque, J., "Experimental Studies of Aluminum Agglomeration in Solid Rocket Motors," *International Journal of Energetic Materials and Chemical Propulsion*, Vol. 4, No. 1-6, 1997,
doi: 10.1615/IntJEnergeticMaterialsChemProp.v4.i1-6.650.

[44] Marble, F. E., "Dynamics of a Gas Containing Small Solid Particles," *Proceedings of the 5th AGARD Combustion and Propulsion Symposium*, Pergamon Press, New York, 1963.

[45] Spalding, D. B., "Combustion of Fuel Particles," *Fuel*, Vol. 30, No. 1, 1951, pp. 121–130.

[46] Godsave, G. A. E., "Studies of the Combustion of Drops in a Fuel Spray–The Burning of Single Drops of Fuel," *Symposium (International) on Combustion*, Vol. 4, No. 1, 1953, pp. 818–830,
doi: 10.1016/S0082-0784(53)80107-4.

[47] Dupays, J., "Two-phase Unsteady Flow in Solid Rocket Motors," *Aerospace Science and Technology*, Vol. 6, No. 6, 2002, pp. 413–422,
doi: 10.1016/S1270-9638(02)01182-3.

[48] Sundaram, D. S., Puri, P., and Yang, V., "A general theory of ignition and combustion of nano-and micron-sized aluminum particles," *Combustion and Flame*, Vol. 169, 2016, pp. 94–109,
doi: 10.1016/j.combustflame.2016.04.005.

[49] Braconnier, A., Chauveau, C., Halter, F., and Gallier, S., "Detailed analysis of combustion process of a single aluminum particle in air using an improved experimental approach," *International Journal of Energetic Materials and Chemical Propulsion*, Vol. 17, No. 2, 2018,
doi: 10.1615/IntJEnergeticMaterialsChemProp.2018027988.

[50] Li, H., Rosebrock, C. D., Wu, Y., Wriedt, T., and Mädler, L., "Single Droplet Combustion of Precursor/Solvent Solutions for Nanoparticle Production: Optical Diagnostics on Single Isolated Burning Droplets with Micro-Explosions," *Proceedings of the Combustion Institute*, 2018,
doi: 10.1016/j.proci.2018.06.133.

[51] Ranz, W. E. and Marshall, W. R., "Evaporation from Drops," *Chemical Engineering Progress*, Vol. 48, No. 3, 1952, pp. 141–146.

[52] Schiller, L. and Naumann, A., "Über die Grundlegenden Berechnungen bei der Schwerkraftaufbereitung," *Zeitschrift Des Vereines Deutscher Ingenieure*, Vol. 77, No. 12, 1933, pp. 318–320.

[53] Durand, P., Vieille, B., Lambare, H., Vuillermoz, P., Boure, G., Steinfeld, P., Godfroy, F., and Guery, J., "CPS-A Three Dimensional CFD Code Devoted to Space Propulsive Flows," AIAA paper 2000-3864, June 2000,
doi: 10.2514/6.2000-3864.

[54] Apte, S. and Yang, V., "A Large-Eddy Simulation Study of Transition and Flow Instability in a Porous-Walled Chamber with Mass Injection," *Journal of Fluid Mechanics*, Vol. 477, 2003, pp. 215–225,
doi: 10.1017/S0022112002002987.

[55] Salita, M., "Quench Bomb Investigation of Al2O3 Formation from Solid Rocket Propellants (Part II): Analysis of Data," *25th JANNAF Combustion Meeting*, 1988, pp. 185–197.

[56] Flandro, G. A., "Effects of Vorticity on Rocket Combustion Stability," *Journal of Propulsion and Power*, Vol. 11, No. 4, 1995, pp. 607–625,
doi: 10.2514/3.23887.

[57] Flandro, G., Cai, W., and Yang, V., "Turbulent Transport in Rocket Motor Unsteady Flowfield," *Solid Propellant Chemistry, Combustion, and Motor Interior Ballistics*, Vol. 185, Progress in Astronautics and Aeronautics, 2000, pp. 837–858, doi: 10.2514/5.9781600866562.0837.0858.

[58] Majdalani, J. and Van Moorhem, W., "Multiple-Scales Solution to the Acoustic Boundary Layer in Solid Rocket Motors," *Journal of Propulsion and Power*, Vol. 13, No. 2, 1997, pp. 186–193, doi: 10.2514/2.5168.

[59] Mikhail, M. N. and El-Tantawy, M. R., "The Acoustic Boundary Layers: a Detailed Analysis," *Journal of Computational and Applied Mathematics*, Vol. 51, No. 1, 1994, pp. 15–36, doi: 10.1016/0377-0427(94)90091-4.

[60] Zhu, M., Dowling, A., and Bray, K., "Self-Excited Oscillations in Combustors with Spray Atomizers," *Journal of Engineering for Gas Turbines and Power*, Vol. 123, No. 4, 2001, pp. 779–786, doi: 10.1115/1.1376717.